Geophysical Journal International

Geophys. J. Int. (2017) **209,** 387–405
Advance Access publication 2017 January 25
GJI Geomagnetism, rock magnetism and palaeomagnetism

doi: 10.1093/gji/ggx023

FDTD modelling of induced polarization phenomena in transient electromagnetics

Michael Commer, Peter V. Petrov and Gregory A. Newman

Lawrence Berkeley Nat'l Lab, Earth and Environmental Sciences Area, 1 Cyclotron Rd., MS 74R316C, Berkeley, CA 94720*, USA. E-mail: MCommer@lbl.gov*

Accepted 2017 January 23. Received 2017 January 17; in original form 2016 October 11

SUMMARY

The finite-difference time-domain scheme is augmented in order to treat the modelling of transient electromagnetic signals containing induced polarization effects from 3-D distributions of polarizable media. Compared to the non-dispersive problem, the discrete dispersive Maxwell system contains costly convolution operators. Key components to our solution for highly digitized model meshes are Debye decomposition and composite memory variables. We revert to the popular Cole–Cole model of dispersion to describe the frequency-dependent behaviour of electrical conductivity. Its inversely Laplace-transformed Debye decomposition results in a series of time convolutions between electric field and exponential decay functions, with the latter reflecting each Debye constituents' individual relaxation time. These function types in the discrete-time convolution allow for their substitution by memory variables, annihilating the otherwise prohibitive computing demands. Numerical examples demonstrate the efficiency and practicality of our algorithm.

Key words: Numerical solutions; Numerical approximations and analysis; Electrical properties; Electromagnetic theory; Marine electromagnetics.

1 INTRODUCTION

In electromagnetic (EM) geophysics, dispersive media is characterized by a frequency dependence of the electrical conductivity. The resulting phenomenon—induced polarization (IP)—has first been recognized as being important in mineral exploration (Pelton *et al.* 1978). More recently, the range of applications has widened considerably because IP effects are often associated with processes occurring in environmental geosciences and hydrogeology (e.g. Revil *et al.* 2014) and petroleum studies (e.g. Schmutz *et al.* 2010). We also refer the reader to, for example, Seigel *et al.* (2007) for a historical overview of the IP method and to Ustra *et al.* (2016) for a comprehensive summary of the current understanding of IP source mechanisms.

A common phenomenological model to describe the frequency dependence of polarization effects is the Cole–Cole model (Pelton *et al.* 1978), to be abbreviated as CCM in the following. Adopting this model in our methodology, we follow the nomenclature of Tarasov & Titov (2013) for formulating the frequency-dependent complex electrical conductivity, measured in units of Siemens per meter (S m^{-1}),

$$\boldsymbol{\sigma}^*(\mathrm{i}\omega) = \boldsymbol{\sigma}_\infty \left(1 - \frac{m}{1 + (\mathrm{i}\omega\tau)^c}\right), \tag{1}$$

where ω denotes the angular frequency and i is the imaginary unit. Further, τ is the CCM parameter central relaxation time and $\boldsymbol{\sigma}_\infty$ defines the high-frequency (inductive) limit of the electrical conductivity. The latter is related to the low-frequency (DC) limit, $\boldsymbol{\sigma}_0$, via the chargeability m, which is a macroscopic physical parameter describing a media's polarization magnitude,

$$m = \frac{\sigma_\infty - \sigma_0}{\sigma_\infty}. \tag{2}$$

In eq. (1), the CCM parameter c is referred to as CCM exponent and accounts for different spectral shapes of the CCM response, in principal describing the broadness of a continuous relaxation time distribution (Tarasov & Titov 2013). This versatility to define relaxation time distributions by means of one parameter may be the prevailing reason for the CCM's popularity.

Geophysical EM modelling methods that incorporate eq. (1) favour the frequency-domain over the time-domain. One reason is the basic fact that the multiplication with a frequency-dependent complex electrical conductivity translates into the time-domain's computationally burdensome convolution counterpart (Tarasov & Titov 2007). Simplified models that infer analytical time-domain solutions can render the straightforward convolution feasible (Smith *et al.* 1988). However, typical cases of Cole–Cole dispersion imply exponents of $c < 1$, causing the appearance of less favourable (in a convolutionary system) fractional derivatives in the time-domain (Wait 1984; Petropoulos 2008). To

circumvent these difficulties, many IP forward modelling algorithms perform a series of frequency-domain calculations which are subsequently converted to the time-domain via Fourier, Laplace or Hankel transforms (e.g. Lee 1981; Flis *et al.* 1989; Fiandaca *et al.* 2012) Advancing the efficiency of this process, Zaslavsky & Druskin (2010) subject the Maxwell system with CCM dispersion to Krylov subspace reduction techniques applied in the frequency domain, with its solutions transformed to the time-domain using numerical integration. Without the availability of the latter type of methods, the calculation of wide frequency bands necessary to cover multiple time decades using standard 3-D finite-difference (FD) or finite-element methods may require hundreds of forward solutions for good enough accuracy (Zaslavsky & Druskin 2010), thus being potentially computationally burdensome.

Explicitly time-stepping fields in dispersive media through the finite-difference time-domain (FDTD) method remains attractive, mostly since it bypasses the numerical complications coming along with bridging the two domains, also since its implementation is relatively straightforward. However, despite its conceptual simplicity, the relevance of FDTD methods to model IP hinges on the ability to efficiently implement convolutionary Maxwell systems. Three classes of techniques target this aspect: (1) recursive convolution (Kelley & Luebbers 1996; Taflove *et al.* 2005), (2) auxiliary differential equations (ADE; Kashiva *et al.* 1990; Taflove *et al.* 2005; Rekanos & Papadopoulos 2010), and (3) Z-transform method (Sullivan 1992a; Weedon & Rappaport 1997). Early applications of these methods treated electrical engineering and biomedical problems with frequency-dependent relative permittivity functions (e.g. Hurt 1985; Luebbers *et al.* 1990; Gandhi *et al.* 1993). Consequently, following geophysical work involved FDTD for ground penetrating radar over dispersive soils (e.g. Teixeira *et al.* 1998).

Our approach treats a time-domain convolutionary Maxwell system using the concept of Debye decomposition, where the frequency-dependent part of eq. (1) is deconvolved into superpositions of low-order Debye dispersion relations (e.g. Hurt 1985; Luebbers *et al.* 1990; Sullivan 1992b). In our case, the elementary polarizing responses are given by a weighted sum of different Debye relaxations ($c = 1$).

Our approach resembles the ADE method, which effectively treats a Cole–Cole medium by approximating it with function expansions that are described by a differential equation with derivatives of integer order. Rekanos & Papadopoulos (2010) implemented an ADE method for FDTD using a Padé approximation of the CCM. Recall that Padé approximants expand a function as a ratio of two power series, resulting in rational series of integer order terms. The latter are easier to convert to the time-domain through the Z-transform method (Wismer & Ludwig 1995; Marchant *et al.* 2014). In our approach we approximate the CCM by a weighted sum of different Debye relaxations. These are just two of several types of CCM approximations that give rise to an ADE. In both cases, one wants to avoid fractional derivatives which correspond to time differentiation of a convolutional integral.

Debye decomposition has some physical basis, because it is believed that IP effects are likely to result from multiple interacting physio-chemical phenomena, causing the superposition of multiple polarization mechanisms (Revil & Florsch 2010). Ustra *et al.* (2016) provide an excellent overview of the developments related to the Debye decomposition of complex electric conductivity spectra. The Debye decomposition further facilitates the adoption of earlier developments in seismological modelling, where we use the fact that the Debye model's simple exponential decay allows for the efficient evaluation of convolutionary integrals by means of composite memory variables (Carcione *et al.* 1988; Carcione 1990; Xu & McMechan 1995).

For the derivation of the FDTD updating scheme for dispersive media, we build upon the parallel explicit FDTD scheme for the diffusive form of Maxwell's equations described in an earlier work (Commer & Newman 2004). The augmented FDTD formulation contains appropriate memory variables that replace auxiliary discrete-time convolution terms. We finally present numerical studies to investigate potential numerical modelling errors and demonstrate the algorithm's usefulness for a wide range of CCM parameters in practical geophysical survey scenarios.

2 METHODOLOGY

Our explicit FD time-stepping procedure involves an alternating update of the magnetic field vectors, given by magnetic field $\mathbf{h}$ and magnetic induction $\mathbf{b}$, and electric field vectors $\mathbf{e}$ in a leap-frog manner (Oristaglio & Hohmann 1984; Wang & Hohmann 1993; Commer & Newman 2004). These fields are spatially discretized on a Cartesian staggered grid approximating arbitrary spatial 3-D electrical conductivity variations within a lossy medium. For completeness, we restate here the basic equation set of the explicit FDTD scheme. It is given by the time-domain Maxwell equations in the diffusive limit,

$$\nabla \times \mathbf{e} + \frac{\partial \mathbf{b}}{\partial t} = 0, \tag{3}$$

$$\nabla \times \mathbf{h} - \boldsymbol{\sigma}\mathbf{e} - \gamma \frac{\partial \mathbf{e}}{\partial t} = \mathbf{j}_s, \tag{4}$$

with $\mathbf{j}_s$ describing the vector of primary electric current density impressed by a transmitting source and γ describing a fictitious permittivity (Oristaglio & Hohmann 1984). Eq. (4) describes a non-dispersive medium, characterized by a time-invariant electrical conductivity tensor $\boldsymbol{\sigma}$. Only diagonal tensor elements are considered, given by the directional edge conductivities along the three Cartesian coordinates.

To understand how eq. (4) changes for dispersive media, recall Ohm's law generalized for the time-dependent current density (e.g. Davydycheva *et al.* 2006)

$$\mathbf{j}(t) = \int_{-\infty}^{t} \boldsymbol{\sigma}(t')\mathbf{e}(t - t')\mathrm{d}t'. \tag{5}$$

Dispersivity in the time-domain turns the electrical current density $\boldsymbol{\sigma}\mathbf{e}$ in eq. (4) into a convolution term, $\mathbf{j}(t) = \boldsymbol{\sigma}(t) * \mathbf{e}(t)$, where $\boldsymbol{\sigma}(t)$ would be replaced by the time-domain version of any phenomenological spectral IP model. In our case, the latter is given by the inverse Laplace

transform of eq. (1), $\mathcal{L}^{-1}\{\boldsymbol{\sigma}^*\}$. Unfortunately, for the general case $c < 1$, this is difficult to obtain, which is basically rooted in the fact that eq. (1) satisfies a fractional order differential equation in the time-domain, rather than a simple ordinary differential equation (Wait 1984; Petropoulos 2008). Considering only the asymptotic behaviour of late-time limits alleviates this problem to a certain degree (Lee 1981). Nonetheless, in either case one is left with Gamma-function series terms (with the exception of the Warburg-form, where $c = \frac{1}{2}$) that would render the evaluation of the convolution integral in eq. (5) extremely computing-intense. Note that the 3-D FDTD scheme would demand to convolve the electric field at every time step and for each cell of a highly digitized FD mesh.

As mentioned in the introduction, various FDTD approaches have used the fact that the numerical convolution becomes feasible for an important special case given by the limit $c \to 1$. Then, the CCM reduces to the Debye model, characterized by a single relaxation time τ_0. For the Debye form, taking the inverse Laplace transform of eq. (1) (with $c = 1$) leads to

$$\mathcal{L}^{-1}\{\boldsymbol{\sigma}^*(\mathrm{i}\omega)\} = \boldsymbol{\sigma}(t) = \boldsymbol{\sigma}_\infty \delta(t) - \frac{\boldsymbol{\sigma}_\infty - \boldsymbol{\sigma}_0}{\tau_0} \exp\left(\frac{-t}{\tau_0}\right) u(t), \tag{6}$$

with $\delta(t)$ and $u(t)$ representing the Dirac delta and Heavyside step functions, respectively.

The electrical current density in dispersive media is now obtained by convolving $\boldsymbol{\sigma}(t)$ with an applied electric field:

$$\mathbf{j}(t) = \boldsymbol{\sigma}(t) * \mathbf{e}(t) = \int_{-\infty}^{t} \boldsymbol{\sigma}_\infty \delta(t - t')\mathbf{e}(t')\mathrm{d}t' + \frac{\boldsymbol{\sigma}_0 - \boldsymbol{\sigma}_\infty}{\tau_0} \int_{-\infty}^{t} \exp\left(-\frac{t - t'}{\tau_0}\right) u(t - t')\mathbf{e}(t')\mathrm{d}t'. \tag{7}$$

Consider now the case of a turn-on source waveform. Because of $\mathbf{e}(t) = 0$ for $t \le 0$, eq. (7) becomes

$$\mathbf{j}_{\mathrm{on}}(t) = \boldsymbol{\sigma}_\infty \mathbf{e}(t) + \frac{\boldsymbol{\sigma}_0 - \boldsymbol{\sigma}_\infty}{\tau_0} \int_0^t \exp\left(-\frac{t - t'}{\tau_0}\right) \mathbf{e}(t')\mathrm{d}t'. \tag{8}$$

Eq. (8) shows the inductive limit for the current density at time zero: $\mathbf{j}_{\mathrm{on}}(t = 0) = \boldsymbol{\sigma}_\infty \mathbf{e}(0)$. For a turn-off source waveform, the electric field before current shutdown is given by a static DC field, $\mathbf{e}(t) = \mathbf{e}_{\mathrm{DC}}$ for $t \le 0$. Then, the current density eq. (8) receives an additional term and becomes

$$\mathbf{j}_{\mathrm{off}}(t) = \boldsymbol{\sigma}_\infty \mathbf{e}(t) + (\boldsymbol{\sigma}_0 - \boldsymbol{\sigma}_\infty) \exp\left(\frac{-t}{\tau_0}\right) \mathbf{e}_{\mathrm{DC}} + \frac{\boldsymbol{\sigma}_0 - \boldsymbol{\sigma}_\infty}{\tau_0} \int_0^t \exp\left(-\frac{t - t'}{\tau_0}\right) \mathbf{e}(t')\mathrm{d}t', \tag{9}$$

which at time zero reduces to $\mathbf{j}_{\mathrm{off}}(t = 0) = \boldsymbol{\sigma}_0 \mathbf{e}_{\mathrm{DC}}$.

2.1 Debye function expansions of complex conductivity

Eqs (8) and (9) show that the Debye-form can be incorporated easily into the explicit FDTD method, owing to the simple exponential decay over time. Further, it has been found that for dispersive materials, one can approximate eq. (1) by a weighted sum of Debye models (Gandhi *et al.* 1993; Wismer & Ludwig 1995; Torres *et al.* 1996; Schuster & Luebbers 1998; Kelley *et al.* 2007; Nordsiek & Weller 2008). Following this approach, eq. (1) translates to

$$\boldsymbol{\sigma}_\infty \left(1 - \frac{m}{1 + (\mathrm{i}\omega\tau)^c}\right) \approx \boldsymbol{\sigma}_\infty + (\boldsymbol{\sigma}_0 - \boldsymbol{\sigma}_\infty) \sum_{i=0}^{N_{\mathrm{Debye}}} \frac{\alpha_i}{1 + (\mathrm{i}\omega\tau_i)}. \tag{10}$$

Since τ_0 describes a (single-term) Debye model, the summation in eq. (10) starts at $i = 0$. The number of Debye models is thus given by $N_{\mathrm{Debye}} + 1$. In other contexts, the summation term in eq. (10) is also referred to as multipole Debye model (e.g. Krewer *et al.* 2013). Each Debye pole, or summand i, is comprised of an individual relaxation time τ_i paired with a weighting coefficient $\alpha_i \in]0, 1]$.

The inverse Laplace transform of each summand in eq. (10) is given by eq. (6), specifically

$$\mathcal{L}^{-1}\left(\frac{\alpha_i}{1 + (\mathrm{i}\omega\tau_i)}\right) = \frac{\alpha_i}{\tau_i} \exp\left(\frac{-t}{\tau_i}\right) u(t),$$

leading to the Debye function expansions for $\mathbf{j}_{\mathrm{on}}(t)$ and $\mathbf{j}_{\mathrm{off}}(t)$:

$$\mathbf{j}_{\mathrm{on}}(t) = \boldsymbol{\sigma}_\infty \mathbf{e}(t) + (\boldsymbol{\sigma}_0 - \boldsymbol{\sigma}_\infty) \sum_{i=0}^{N_{\mathrm{Debye}}} \frac{\alpha_i}{\tau_i} \int_0^t \exp\left(-\frac{t - t'}{\tau_i}\right) \mathbf{e}(t')\mathrm{d}t', \tag{11}$$

$$\mathbf{j}_{\mathrm{off}}(t) = \boldsymbol{\sigma}_\infty \mathbf{e}(t) + (\boldsymbol{\sigma}_0 - \boldsymbol{\sigma}_\infty) \sum_{i=0}^{N_{\mathrm{Debye}}} \frac{\alpha_i}{\tau_i} \int_0^t \exp\left(-\frac{t - t'}{\tau_i}\right) \mathbf{e}(t')\mathrm{d}t' + (\boldsymbol{\sigma}_0 - \boldsymbol{\sigma}_\infty)\mathbf{e}_{\mathrm{DC}} \sum_{i=0}^{N_{\mathrm{Debye}}} \alpha_i \exp\left(\frac{-t}{\tau_i}\right). \tag{12}$$

We define a pure Debye medium by $N_{\mathrm{Debye}} = 0$, involving only one relaxation time, τ_0 with $\alpha_0 = 1$. Then, eqs (11) and (12) revert to eqs (8) and (9).

Fitting a series of decaying exponentials to a given CCM involves an optimization problem to estimate suitable parameter coefficient pairs (α_i, τ_i) for eqs. (11) and (12) that satisfy eq. (10). This problem can be reduced to a least-squares minimization of the expansion error ε in

$$\frac{1}{1 + (\mathrm{i}\omega\tau)^c} = \sum_{i=0}^{N_{\mathrm{Debye}}} \frac{\alpha_i}{1 + (\mathrm{i}\omega\tau_i)} + \varepsilon. \tag{13}$$

Least-squares optimization has commonly been used for this kind of problem, usually for the estimation of multiterm Debye dispersion relations for permittivity (e.g. Sheppard 1973; Hurt 1985), also in the context of frequency-dependent seismic wave attenuation (Emmerich & Korn 1987). Unfortunately, this approach does not guarantee stable FDTD results because of the instances where a solution may produce negative relaxation times τ_i, leading to an exponential growth of the convolution terms in eqs (11) and (12). Global search methods (Krewer *et al.* 2013) or their combination with least-squares approaches (Kelley *et al.* 2007) have thus been proposed. Our approach stays with a regular least-squares optimization method provided by the toolbox MINPACK (Moré *et al.* 1984). While this is understood not to be optimal, we have found it to be satisfactory for a range of CCM parameters that may cover a significant spectrum of practical applications as will be demonstrated by numerical examples later.

Regarding computing effort, each unique CCM τ, c-combination in a 3-D model with inhomogeneous distribution of polarizable media represents a separate least-squares problem. We employ a so-called 'embarassingly-parallel' approach to solve multiple least-squares problems independently.

2.2 Estimating the accuracy of Debye function expansions

A series of curve-fitting attempts is carried out in the following in order to quantify the goodness of fit achieved by multipole Debye models that minimize the error ε in eq. (13). In Fig. 1, the CCM exponent c is varied from $c = 0.75$ down to $c = 0.10$. For each CCM, multiple realizations of eq. (13), defined by the degrees $N_{\text{Debye}} = 1, 2, \ldots, 7$, are solved for coefficient estimates α_i, τ_i (with $i = 0, \ldots, N_{\text{Debye}}$). The CCM relaxation time remains constant at τ =1 sec. We have identified two measures that appear suitable for assessing the quality of fit. First, the quantity

$$q_1 = \left| 1 - \sum_{i=0}^{N_{\text{Debye}}} \alpha_i \right| \tag{14}$$

uses the fact that a departure from $\sum_{i=0}^{N_{\text{Debye}}} \alpha_i = 1$ indicates a deteriorated fit, which can be seen from considering the limit $\omega \to 0$, where eq. (13) must become $\varepsilon = 0$; otherwise $\boldsymbol{\sigma}_\infty(\omega = 0) = \boldsymbol{\sigma}_0$ would not hold in eq. (10). In the other limit $\omega \to \infty$, q_1 becomes a limit for the maximum approximation accuracy that can be reached by eq. (10).

The concrete examples for the CCM parameter c in Fig. 1 highlight two aspects. First, for the cases $c = 0.75$, $c = 0.5$ and $c = 0.25$, the general trend of q_1 towards zero correlates well with the increased degree of freedom given by N_{Debye}. Note that for $c = 0.75$, q_1 already indicates an insignificant fitting error for $N_{\text{Debye}} \geq 2$. Second, a decreasing c aggravates the curve-fitting process, which eventually fails at $c = 0.1$, where all outcomes for q_1 remain rather high.

A second quality measure is given by the ratio

$$q_2 = \frac{\varepsilon_I}{\varepsilon_0}, \tag{15}$$

representing the relative misfit decrease between the initial guess and the final least-squares iteration I, both calculated from eq. (13). For $c \geq 0.25$, one observes a general correlation between q_1 and q_2, pointing out a minimal fitting error ε_I for the largest number of Debye poles $N_{\text{Debye}} = 7$.

It is further of interest to visualize the actual fitting of both the real and imaginary components of the left-hand-side of eq. (13). These components are annotated as CCM (black and grey curves) in Fig. 2 for the CCM examples $c = 0.75$ and $c = 0.25$. Their respective approximations given by the right-hand-side of eq. (13) are annotated as Debye (blue and brown curves). As both quantities q_1 and q_2 already indicated, an increasing number N_{Debye} delivers an increasing goodness of fit for both instances of c. Furthermore, a lower CCM exponent aggravates the fitting by exponential functions, because for $c = 0.25$ the actual CCM function owns a more flattened decay than for $c = 0.75$. This explains why the curve-fitting fails for the extreme case of $c = 0.1$ shown in Fig. 1, where both fitting measures q_1 and q_2 indicate a rather poor fit for all attempted realizations of Debye poles N_{Debye}.

Here, we focus on the variation of the CCM exponent c by assuming a constant relaxation time of $\tau = 1$ s. We observed that c has a larger influence than τ on the ability to obtain a satisfactory Debye-series model. Moreover, we observed the general trend that τ, c-combinations that infer a flat CCM function behaviour as exemplified by the case $c = 0.25$ (Fig. 2), lead to deteriorated curve-fitting outcomes. Marchant *et al.* (2014) report a similar issue when representing the CCM's frequency spectrum with Padé approximants. Very low CCM exponents thus require more advanced optimization procedures (Kelley *et al.* 2007; Krewer *et al.* 2013). On the other hand, typical CCM exponents range from 0.2 to 1 (Tarasov & Titov 2013). Given these considerations, we restrict the numerical examples in this work to CCM exponents $c \geq 0.25$.

2.3 FDTD updating equations for dispersive media

With a way of determining Debye-series parameters α_i, τ_i for eqs (11) and (12) in place, the FDTD time-stepping procedure associated with eqs (3) and (4) can now be augmented for polarizable media. One leap-frog cycle of the FDTD scheme involves first updating magnetic fields from the discrete form of eq. (3) and subsequently updating electric fields using the discrete form of eq. (4) (Wang & Hohmann 1993). Hence,

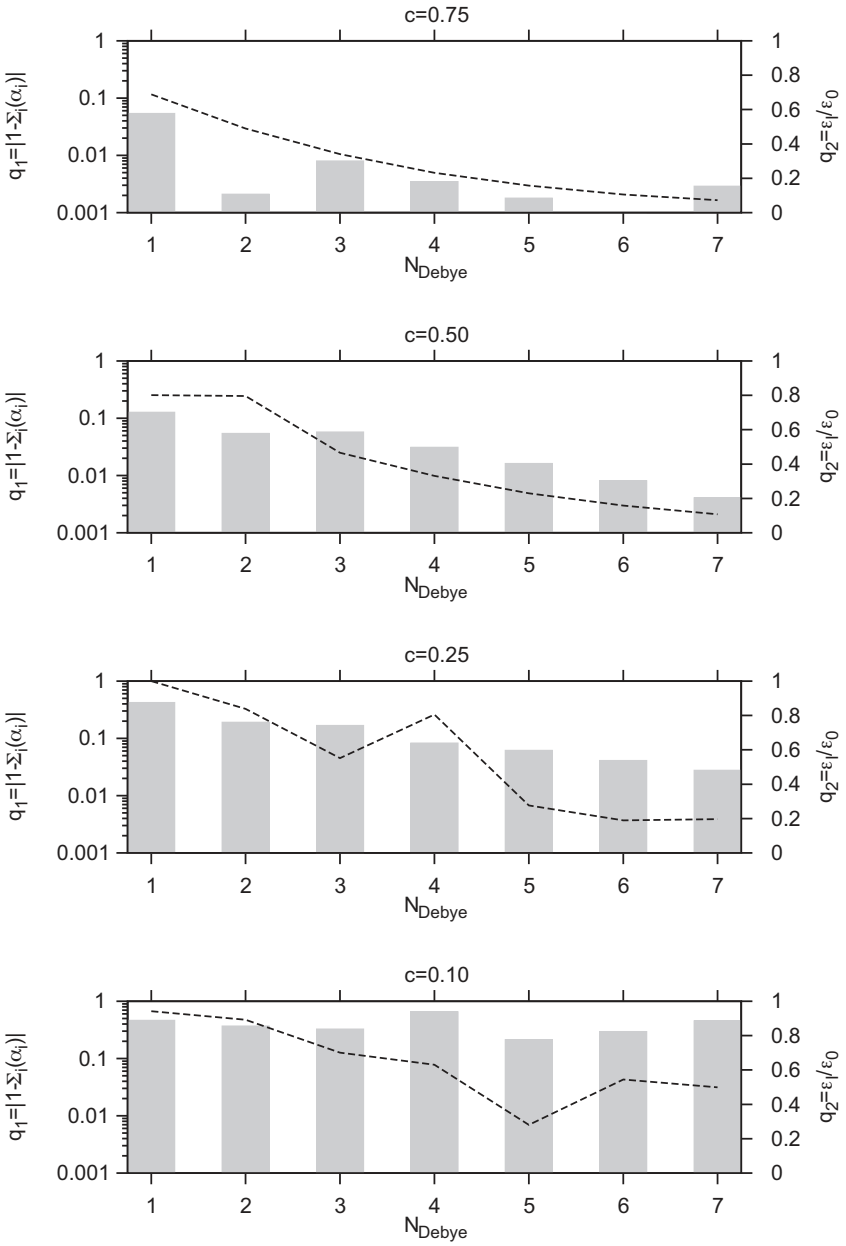

Figure 1. Estimation of the goodness of fit between CCM and a multipole Debye model (eq. 13). Each CCM is distinguished by a different c-parameter, where $\tau = 1$ s is constant, and is matched by Debye series with increasing number of poles $N_{\text{Debye}} = 1, \ldots, 7$. The two quality measures for the curve-fitting process are q_1, shown by the bar graphs, and q_2 (dashed lines), the relative misfit decrease with respect to the initial guess, as reported by MINPACK and normalized here by the maximum of all realizations.

for the dispersive case, only the electric field's updating equation adopts additional expressions through the convolution terms in eq. (7). We first restate the discrete electric-field update for non-dispersive media, defined by $\boldsymbol{\sigma}_\infty = \boldsymbol{\sigma}_0$, where both eqs (8) and (9) reduce to $\mathbf{j}(t) = \boldsymbol{\sigma}\,\mathbf{e}(t)$, leading to (Commer & Newman 2004)

$$\mathbf{e}^{n+1} = \frac{2\gamma - \boldsymbol{\sigma}\,\Delta t}{2\gamma + \boldsymbol{\sigma}\,\Delta t}\mathbf{e}^n + \frac{2\Delta t}{2\gamma + \boldsymbol{\sigma}\,\Delta t}\left(\nabla \times \mathbf{h}^{n+\frac{1}{2}} - \mathbf{j}_s^{n+\frac{1}{2}}\right). \tag{16}$$

Recall that only diffusive fields are considered; hence the displacement term γ is fictitious and does not involve any frequency dependence. With the magnetic-field $\mathbf{h}$ given at half time steps $n + \frac{1}{2}$, the electric field is advanced from the time step n at time t^n to the next step $n + 1$ at time $t^{n+1} = t^n + \Delta t$. For a chargeable medium, the final electric field's updating equation is obtained by inserting the convolution term eq. (7) into Ampere's law (eq. 4). The derivation is outlined in detail in appendix A1. The final formulas are shown here, first for the turn-on source waveform, which involves replacing the current density terms in eq. (16) by the discrete-time convolution expression eq. (8), that is,

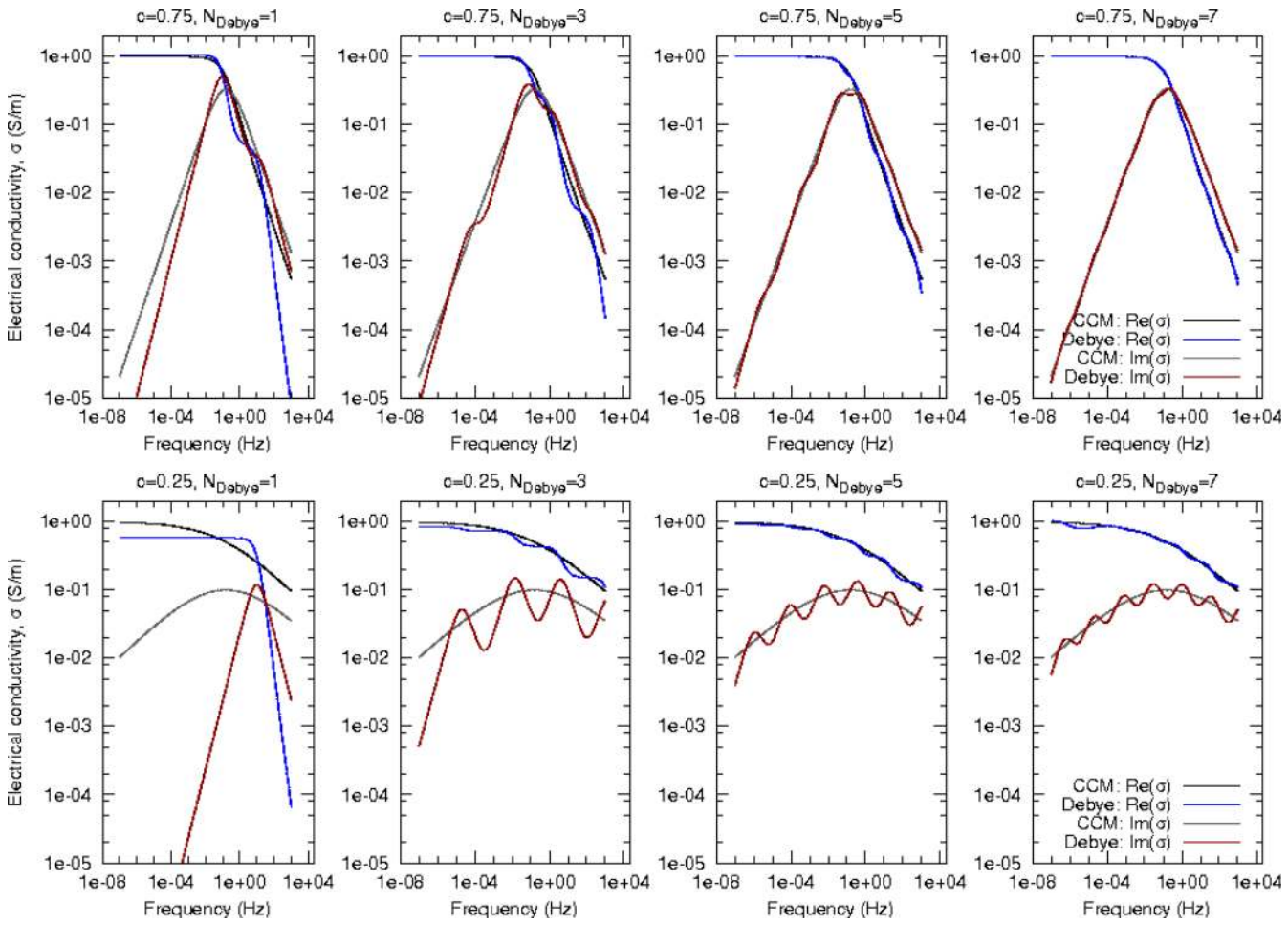

Figure 2. Frequency-domain representation of two CCMs (upper row: $c = 0.75$, lower row: $c = 0.25$, with constant $\tau = 1$ s). Each subplot shows the real and imaginary components of the frequency-dependent electrical conductivity calculated from the actual CCM and their corresponding Debye-series approximations. For the latter, the instances $N_{\text{Debye}} = 1,3,5$, and 7 (eq. 13) are realized (plotted from left to right).

its Debye-series analogue eq. (11):

$$\mathbf{e}^{n+1} = \left\{ \mathbf{e}^n \left[\frac{\gamma}{\Delta t} - \frac{\boldsymbol{\sigma}_\infty}{2} + \frac{\boldsymbol{\sigma}_\infty - \boldsymbol{\sigma}_0}{4} \Delta t \sum_{i=0}^{N_{\text{Debye}}} \frac{\alpha_i}{\tau_i} \exp\left(-\frac{\Delta t}{\tau_i}\right) \right] + \frac{\boldsymbol{\sigma}_\infty - \boldsymbol{\sigma}_0}{2} \sum_{i=0}^{N_{\text{Debye}}} \frac{\alpha_i}{\tau_i} M_i^n \left[1 + \exp\left(-\frac{\Delta t}{\tau_i}\right) \right] + \nabla \times \mathbf{h}^{n+\frac{1}{2}} - \mathbf{j}_s^{n+\frac{1}{2}} \right\} \Big/ \left(\frac{\gamma}{\Delta t} + \frac{\boldsymbol{\sigma}_\infty}{2} - \frac{\boldsymbol{\sigma}_\infty - \boldsymbol{\sigma}_0}{4} \Delta t \sum_{i=0}^{N_{\text{Debye}}} \frac{\alpha_i}{\tau_i} \right). \tag{17}$$

Similarly, the turn-off source waveform employs eq. (12), leading to

$$\mathbf{e}^{n+1} = \left\{ \mathbf{e}^n \left[\frac{\gamma}{\Delta t} - \frac{\boldsymbol{\sigma}_\infty}{2} + \frac{\boldsymbol{\sigma}_\infty - \boldsymbol{\sigma}_0}{4} \Delta t \sum_{i=0}^{N_{\text{Debye}}} \frac{\alpha_i}{\tau_i} \exp\left(-\frac{\Delta t}{\tau_i}\right) \right] + \mathbf{e}_{\text{DC}} \frac{\boldsymbol{\sigma}_\infty - \boldsymbol{\sigma}_0}{2} \left[\sum_{i=0}^{N_{\text{Debye}}} \alpha_i \exp\left(-\frac{t^{n+1}}{\tau_i}\right) + \alpha_i \exp\left(-\frac{t^n}{\tau_i}\right) \right] + \frac{\boldsymbol{\sigma}_\infty - \boldsymbol{\sigma}_0}{2} \sum_{i=0}^{N_{\text{Debye}}} \frac{\alpha_i}{\tau_i} M_i^n \left[1 + \exp\left(-\frac{\Delta t}{\tau_i}\right) \right] + \nabla \times \mathbf{h}^{n+\frac{1}{2}} - \mathbf{j}_s^{n+\frac{1}{2}} \right\} \Big/ \left(\frac{\gamma}{\Delta t} + \frac{\boldsymbol{\sigma}_\infty}{2} - \frac{\boldsymbol{\sigma}_\infty - \boldsymbol{\sigma}_0}{4} \Delta t \sum_{i=0}^{N_{\text{Debye}}} \frac{\alpha_i}{\tau_i} \right). \tag{18}$$

In eqs (17) and (18), the term M_i^n represents the convolution integral

$$M_i^n = M_i(t^n) = \int_0^{t^n} \exp\left(-\frac{t^n - t'}{\tau_i}\right) \mathbf{e}(t') \mathrm{d}t' \tag{19}$$

for a given relaxation time τ_i. The summation terms $\sum_{i=0}^{N_{\text{Debye}}} \frac{\alpha_i}{\tau_i}(\cdots)$ reflect the fact that we compose a Cole–Cole continuous relaxation model, given by $c \in]0, 1]$, of a weighted series of decaying exponentials, where each constitutes a Debye model characterized by its relaxation time τ_i and a corresponding weighting coefficient $\alpha_i \in]0, 1]$. Recall that $N_{\text{Debye}} = 0$ represents a Debye medium, where eqs (17) and (18) involve only one relaxation time τ_0.

2.4 Composite memory variables to replace time convolutions

The convolution in eq. (19) represents a long-time memory requiring storage of the electric field over the whole Cartesian mesh at every time step n. Note that typical transient EM (TEM) simulations involve on the order of 10^4 to 10^5 time steps, where each time step calls for the recomputation of $M_i(t^n)$. Moreover, the summation over N_{Debye} implies multiple convolution integrals, as each is characterized by a different exponential decay τ_i. Realistic models would thus put high demands on current computing resources. To demonstrate, we carried out a FDTD simulation with an implementation of the actual discrete-time convolution in order to compute a four-pole Debye model ($N_{\text{Debye}} = 3$). For a marine TEM standard model (to be introduced below in Section 3), the electric field calculation over the interval (in seconds) $[10^{-2}, 10^2]$ required 50 897 time steps, with an initial time step of $\Delta t = 1.2 \times 10^{-4}$ s. Further, the spatial discretization involved a Cartesian mesh of size $62 \times 62 \times 59$ cells. Utilizing 125 CPU cores of a compute cluster with Intel(R) Xeon(R) (at 2.60 GHz) architecture, the convolution implementation required 84.2 hr to finish. The field storage that comes along with the time integration eq. (19) over the whole mesh amounts to 186 Gigabytes of computer memory. The usage of composite memory variables, to be outlined in the following, reduces these benchmarks to a runtime of 1.1 min and 0.02 Gigabytes of memory.

Replacing the discrete-time convolution between electric field and exponential decay function of each Debye constituent i introduces a corresponding memory variable. Since it replaces the convolution in eq. (19), this memory variable shall also be named M_i in the following. Before the beginning of the time-stepping procedure, the variable initializes to $M_i(t^0 = 0) = 0$. It represents an accumulation term which can be approximated by a first-order Taylor series of eq. (19). At a given time step n, its update to the subsequent time step $n + 1$ is then

$$M_i(t^{n+1}) = M_i(t^n) + \frac{\mathrm{d}}{\mathrm{d}t} M_i(t^n) \Delta t, \tag{20}$$

with the interval $\Delta t = t^{n+1} - t^n$. The time-derivative of eq. (19) can be evaluated through the relationship (Abramowitz & Stegun 1972)

$$\frac{\mathrm{d}}{\mathrm{d}t} \int_{a(t)}^{b(t)} f(t', t) \mathrm{d}t' = \int_{a(t)}^{b(t)} \frac{\partial}{\partial t} f(t', t) \mathrm{d}t' + f(b, t) \frac{\mathrm{d}b}{\mathrm{d}t} - f(a, t) \frac{\mathrm{d}a}{\mathrm{d}t},$$

where $a(t) = 0$, $\frac{\mathrm{d}}{\mathrm{d}t} a(t) = 0$, $b(t) = t^n$, and $f\big(b(t), t\big) \frac{\mathrm{d}}{\mathrm{d}t} b(t) = \mathbf{e}(t^n) = \mathbf{e}^n$, yielding

$$\begin{aligned} M_i(t^{n+1}) &= M_i(t^n) + \left[-\frac{1}{\tau_i} \int_0^{t^n} \exp\left(-\frac{t^n - t'}{\tau_i} \right) \mathbf{e}(t') \mathrm{d}t' + \mathbf{e}(t^n) \right] \Delta t \\ &= M_i(t^n) \left(1 - \frac{\Delta t}{\tau_i} \right) + \mathbf{e}(t^n) \Delta t. \end{aligned} \tag{21}$$

Note that M has units of a time-integrated electric field, i.e. $[M] = [E][t]$. With this implementation, a multipole Debye model essentially reduces to a set of memory variables M_i ($i = 0, \ldots, N_{\text{Debye}}$). In terms of computing effort, their update at each time step compares to the field update eq. (16).

3 NUMERICAL MODEL STUDIES

The purpose of the presented modelling studies is twofold. First, given the popularity of the CCM, we want to shed some light onto the effect that CCM parameters have on the decay behaviour of TEM signals. Second, it is important to assess the accuracy one can expect from approximating an arbitrary CCM by a Debye series. The latter purpose exposes another aspect: while the CCM may be well established as a versatile approximation of a profoundly complicated natural process that has yet to be fully understood, the actual realization of this simple model can be hampered by inherent numerical difficulties. In our case, these difficulties arise from the inverse Laplace transformation of the simple frequency-dependent function in eq. (1). Reference solutions for our FDTD calculations should therefore be obtained in the frequency domain, before transforming into the time-domain. To do so, we employ the standard numerical approach of computing Hankel-transforms through a digital filter method (Chave 1983). The semi-analytical algorithm using this technique has already helped us to verify FDTD simulations from another challenging context, which involved TEM fields over extreme electrical conductivity contrasts due to steel casing (Commer *et al.* 2016). Because this case showed good agreement between FDTD and Hankel-transform solutions, we consider the latter method as a reliable source of reference for the present modelling challenge.

3.1 IP effect on transient EM measurements

In a marine TEM modelling context, Holten *et al.* (2010) report that the IP effect diminishes quickly with offset. They further observe a more pronounced influence in shallow waters, as opposed to deep-water surveys. Consequently, for its relevance to a range of practical exploration scenarios, we employ a standard model of a marine TEM survey in shallow water (Fig. 3). Below the seabed, the medium is homogeneous and exhibits dispersive behaviour. To qualitatively categorize the deviation of the TEM decay from the non-dispersive case, 18 transients are calculated for the combinations of the IP parameters m, τ, and c, with $m = 0.05$, 0.1 and 0.2, $\tau = 1$ and 10, $c = 1$, 0.5 and 0.25.

Fig. 4 shows the near-offset responses, where the in-line horizontal electric field due to a horizontal electric dipole transmitter with step-off source waveform is measured at 300 m distance from the source. For all examples, the general observation holds that the degree of late-time decay retardation, measured by voltage levels that are elevated with respect to the non-dispersive case, increases with both chargeability (m) and relaxation time (τ). Compared to the other cases, the Debye model (a) shows a differentiation with relaxation time.

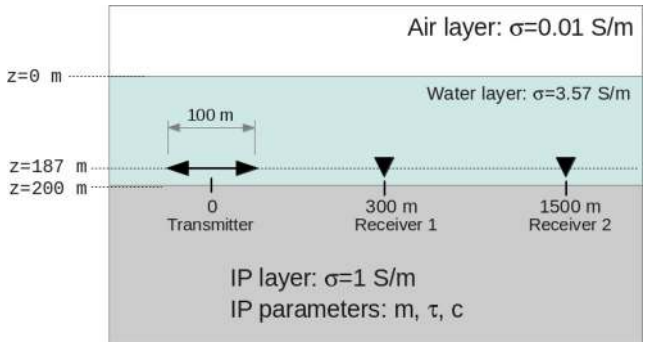

Figure 3. Marine shallow-water TEM standard model with a dispersive seabed, described by the CCM parameters m, τ and c. A horizontal electric dipole transmitter located above the seabed generates in-line TEM fields.

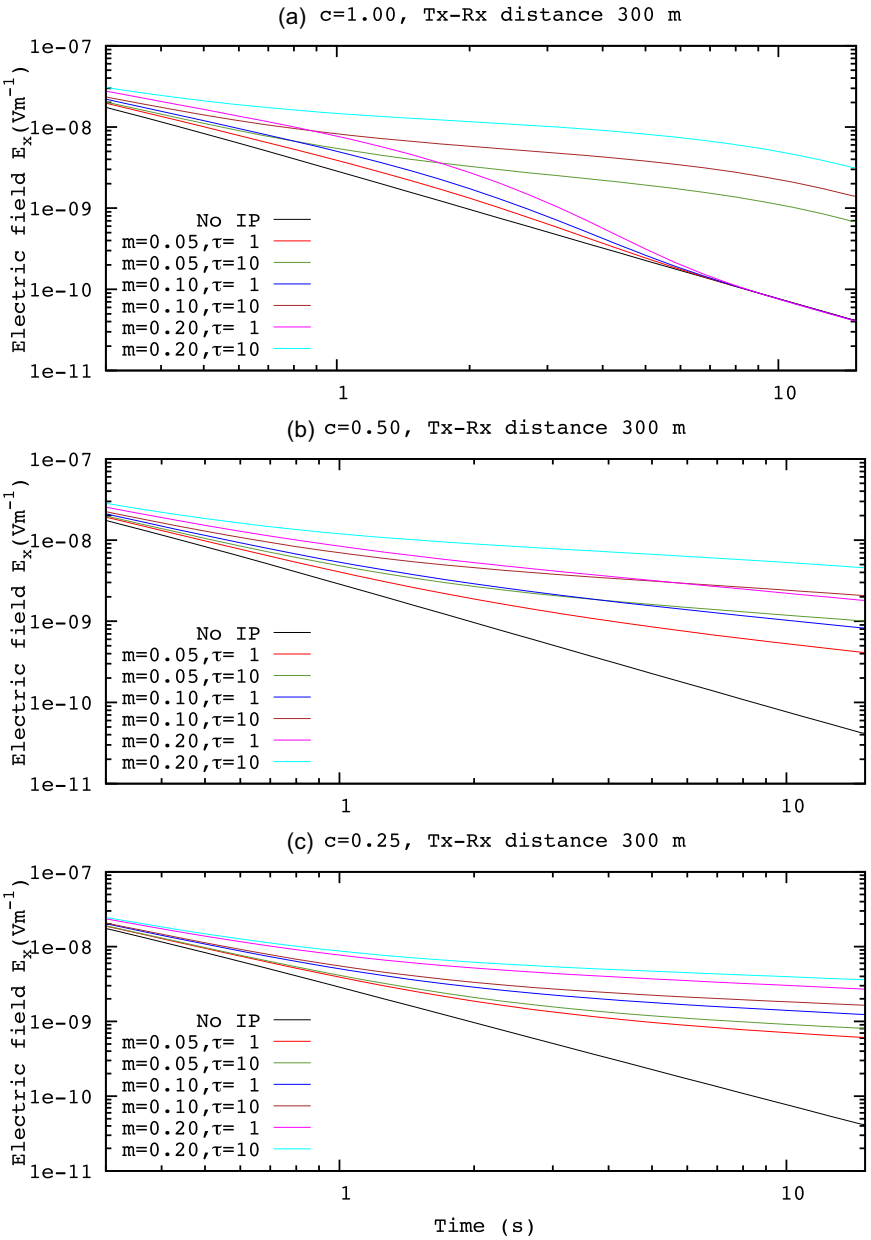

Figure 4. Near-field (Receiver 1) horizontal electric field responses for the marine TEM standard model of Fig. 3. The transients exemplify the IP response compared to the non-dispersive (No IP) case for the CCM exponents (a) $c = 1$, (b) $c = 0.5$ and (c) $c = 0.25$, where each instance employs the same set for the chargeability (m) and relaxation time (τ) parameters.

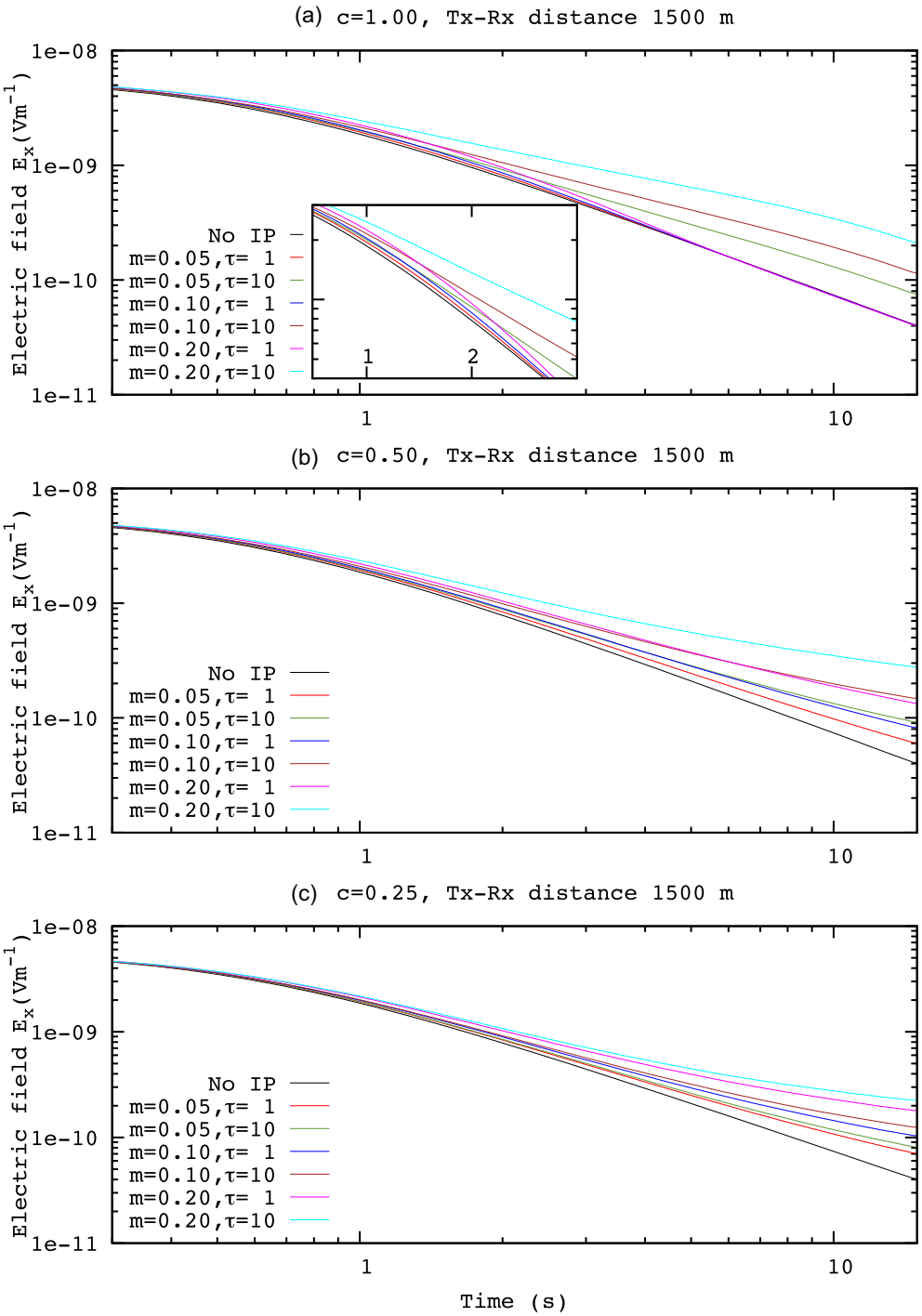

Figure 5. Far-field (Receiver 2) horizontal electric field responses for the marine TEM standard model of Fig. 3. The transients exemplify the IP response compared to the non-dispersive (No IP) case for the CCM exponents (a) $c = 1$, (b) $c = 0.5$ and (c) $c = 0.25$, where each instance employs the same set for the chargeability (m) and relaxation time (τ) parameters.

Transients pertaining to $\tau = 1$ s exhibit a slow-down of the decay occurring only in the mid-time range, whereas for $\tau = 10$ s it prevails over the whole transient length of 15 seconds modelled here. This differentiation with respect to τ vanishes for the other two cases (panels b and c in Fig. 4). Now, increased voltages (compared to the non-IP case shown by the black curve) are measured over the whole time range. For the case $c = 0.25$ (Fig. 4c), the decay attains a similarly slow rate for all combinations of m and τ considered here. Compared to the previous cases (a and b), this leads to the largest degree of resemblance among all transients.

The same IP parameter combinations are modelled in Fig. 5, now for a receiver distance of 1500 m. Qualitatively, the deviations from the non-dispersive response are similar to their near-offset counterparts (Fig. 4), yet with diminished magnitude. In other words,

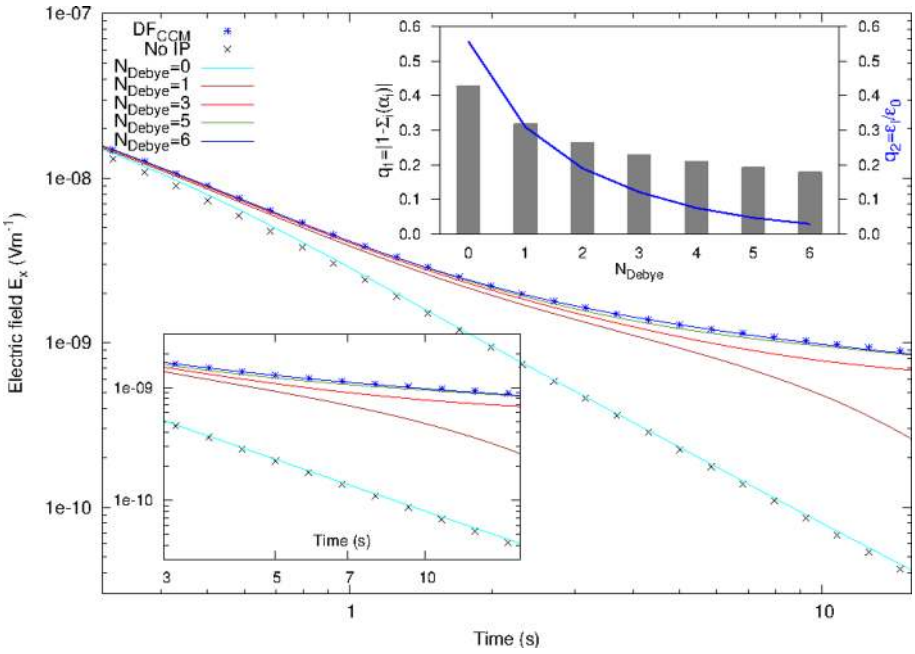

Figure 6. TEM signals for a near-offset horizontal electric field calculated for the marine shallow-water TEM standard model of Fig. 3. The transients generated by multiple Debye-series approximations, with N_{Debye} ranging from 0 (one Debye pole) to 6 (7 poles), are shown in comparison with the reference transient (DF_{CCM}) calculated from a CCM with $m = 0.2$, $\tau = 10$ s, $c = 0.25$. The bar-graph subplot further summarizes the two quality measures q_1 and q_2 resulting from the CCM curve fitting procedure.

the relation of the transients to each other in terms of amplitude differences to the non-IP case remains the same as observed for the near-offset responses.

3.2 TEM signal accuracy dependence on number of Debye poles

The following study to be carried out with the standard model of Fig. 3 inspects how the goodness of fit of the Debye-series approximation correlates with the number of Debye poles N_{Debye}. For this purpose, Fig. 6 summarizes the transient E_x-field of a near-offset position generated by different multipole Debye models, where N_{Debye} varies from 0 to 6; note that this corresponds to 1 to 7 summands in eqs (11) and (12). The CCM to be approximated by Debye series has the parameters $m = 0.2$, $\tau = 10$ s, and $c = 0.25$, causing a relatively strong IP effect in the transient's late time regime. This CCM reference, annotated as DF_{CCM}, was produced by the aforementioned semi-analytical frequency-domain method with a digital-filter solution.

Generally, an increasing N_{Debye} leads to a convergence of the Debye-series transients towards the reference. Interestingly, with a strongly limited degree of freedom, by allowing only one Debye pole ($N_{\text{Debye}} = 0$), the curve-fitting produces the set of parameters $\alpha_0 = 0.57$ and $\tau_0 = 3.5$ s, which lead to an approximation of the non-dispersive transient (annotated as 'No IP'). Instead, one could have assumed a 'true' Debye model, given by $\alpha_0 = 1$, as the best fit. Investigating this a bit further, we found that a transient produced by the parameters $\alpha_0 = 1$ and $\tau_0 = 10$ s deteriorates the fit of the CCM transient in the mid-time range, which hence might have more control over the parameter estimation process.

Adding another Debye pole ($N_{\text{Debye}} = 1$), the strong transient decay retardation of this CCM case becomes better approximated, yet the decay at the latest time still resembles the non-dispersive case. With more Debye poles, the Debye-series transients eventually reflect the true CCM behaviour. The bar-graph subplot highlights the dependence of the quality measures q_1 and q_2, given by eqs. (14) and (15), upholding a similar trend as already observed in Fig. 1: Both measures q_1 and q_2 indicate a better CCM approximation when more Debye poles are added.

3.3 Approximation of far-offset CCM effects by a Debye model

The dispersive transient decay has a certain non-uniqueness aspect: Different IP parameter combinations can lead to similar decay rates, as for example in Fig. 5(b) for the pair $m = 0.05$, $\tau = 10$ (green curve) and $m = 0.1$, $\tau = 1$ (dark blue curve). Low signal-to-noise ratios in actual recordings could render such differences as not discernible. This observation raises the interesting question as to what degree a transient due to an arbitrary CCM ($c < 1$) can be approximated by that of a single Debye model (with constant $c = 1$, but a different m, τ parameter set). Given the implications for inverse applications, where it would be highly desirable to employ only the simplest phenomenological model, we investigate this aspect through curve-fitting.

Considered for this experiment are all far-offset non-Debye transients as shown in Figs 5(b) and (c), because they exhibit a common decay behaviour, while the IP effect is still appreciable. The idea is that some hypothetical survey scenario may require staying within a certain

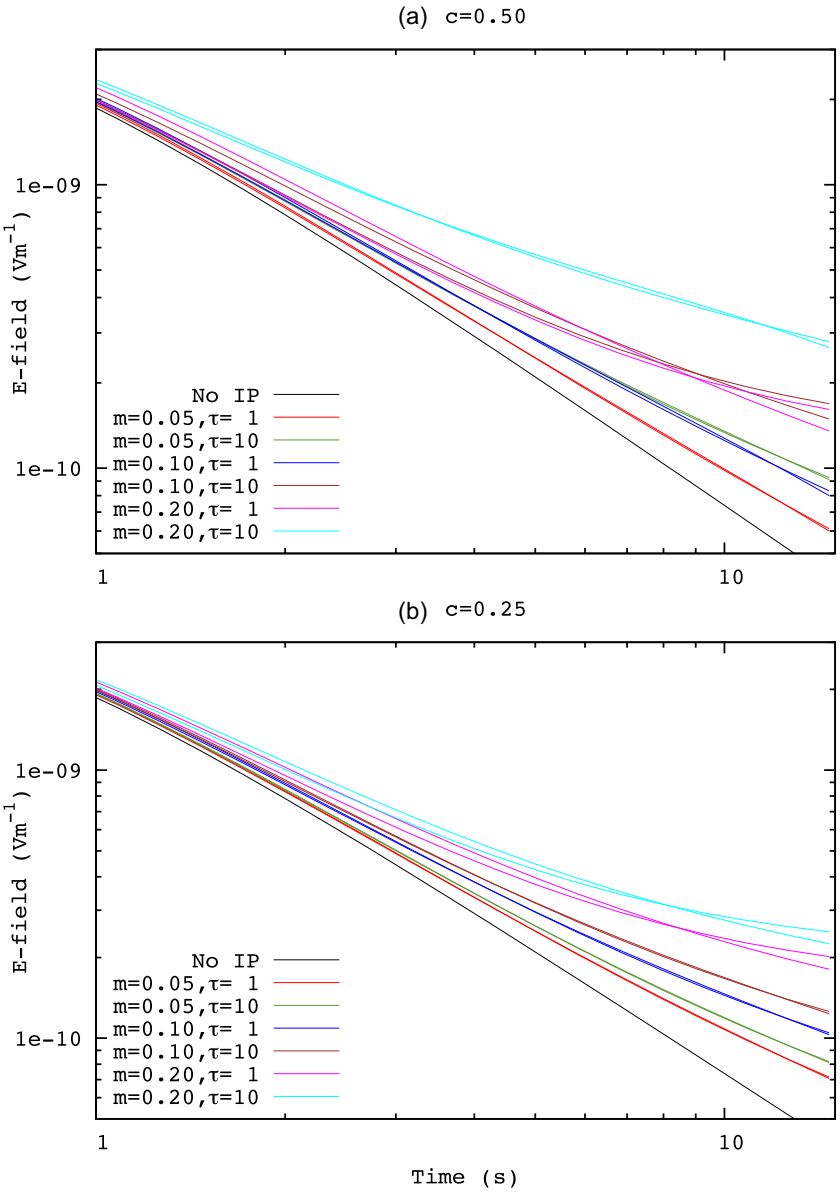

Figure 7. Zoom-in view of transients measured over the dispersive TEM standard model of Fig. 3. Each colour involves a curve pair, where one curve is generated by the original CCM and the second one by a single-Debye-model approximation. Note that towards early times, all transients converge as can be seen in Fig. 5.

distance to the actual target in order to maintain sensitivity, though this distance may be too small to avoid IP effects. As a compromise, one would strive for those distances where IP effects are at least reduced in terms of modelling complexity.

We found that the popular Levenberg–Marquardt optimization method is not the optimal choice for this kind of curve-fitting, owing to the transients' exponential decay. A more robust method for this problem is the Nelder–Mead simplex method (Nelder & Mead 1965), which is offered by the optimization toolbox LMFIT (Newville *et al.* 2014). Fig. 7 summarizes the outcome of the curve-fitting for the transients pertaining to (a) $c = 0.5$ (as also shown in Fig. 5b) and the ones pertaining to (b) $c = 0.25$ (as also shown in Fig. 5c). Each m, τ-parameter combination involves a curve pair of the same colour, with the first curve given by the transient due to the actual CCM and the second curve given by that of a Debye model, where the parameter pair m, τ (with a fixed $c = 1$) is estimated through the Nelder–Mead method.

Table 1 summarizes the m, τ-estimates for each of the 12 IP parameter combinations, also providing estimation errors reported by LMFIT. A general observation is that the curve-fitting tends to be more successful, indicated by low fitting errors, for all those CCM m, τ-combinations that lead to transients approaching the non-dispersive case. Visually, these transients show a large degree of overlap with their respective Debye-model approximations, given in Fig. 7 by all red, green, and blue curve pairs, as well as the brown pair for $c = 0.25$. Further, coinciding with large τ-estimates are large fitting errors of up to two orders of magnitude above the lowest fitting errors, where the latter are achieved for the cases $m = 0.05$. Chargeability estimates appear less variable. While it is likely that the optimization procedure for these instances can be improved, for example by using other minimizers or a combination thereof, this shall not be pursued further. However,

Table 1. Approximation of the CCM by corresponding Debye models with one pole. For each of the CCM m, τ-parameter combinations in the left two columns, far-field transient signals (at Receiver 2) are calculated from the standard model of Fig. 3. A curve-fitting method fits this reference data by transients produced from a Debye model with the estimated parameters and misfit errors reported in columns 3–8. This process is carried out for two CCMs, with $c = 0.5$ (columns 3–5) and $c = 0.25$ (columns 6–8).

True Cole–Cole model parameters		Debye model approximation ($c = 1$ constant)					
		For true CCM with $c = 0.50$			For true CCM with $c = 0.25$		
m	τ	m	τ_0	Error	m	τ_0	Error
0.05	1	0.0162	15.88	3.77	0.0163	30.97	1.20
0.05	10	0.0316	23.37	2.44	0.0204	36.70	1.57
0.10	1	0.0353	14.68	13.11	0.0340	30.16	4.22
0.10	10	0.0527	1848.27	106.90	0.0424	34.49	5.78
0.20	1	0.049	1820.93	296.09	0.0782	2700.41	87.3
0.20	10	0.1394	20.73	15.87	0.1080	3026.23	76.62

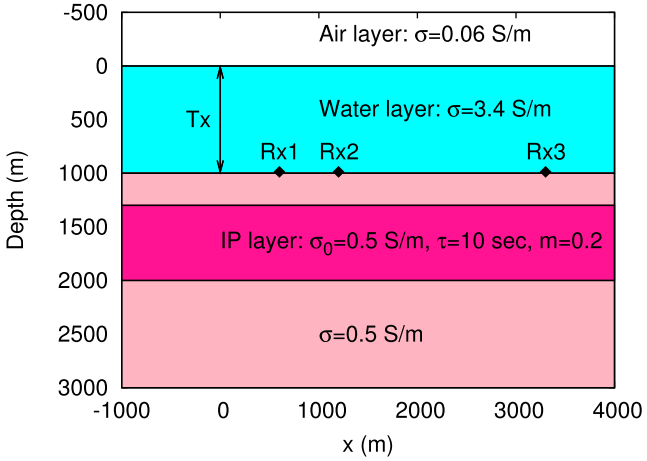

Figure 8. Marine deep-water 1-D model with a vertical electric dipole transmitter and a dispersive layer extending over the depth range 1300–2000 m.

these results let us safely conclude that weak late-time transient IP effects can be approximated to some first-order degree by equivalent (one-pole) Debye models. For the CCM examples considered here, the corresponding Debye parameters are a generally lower chargeability and an elevated, with respect to the true CCM, relaxation time.

3.4 Marine 1-D deep-water model with vertical transmitter

We simulate the IP effect due to a layer with dispersive conductivity in a marine deep-water scenario. In the survey depicted in Fig. 8, the vertical electric field component generated by a vertically oriented electric dipole of 1 km length is measured at the sea bottom. Three ocean-bottom receivers are located at 1 km below sea level. This transmitter type, as opposed to horizontal transmitter dipoles, has the advantage of providing higher sensitivity to deep resistive targets (Holten *et al.* 2009). The vertical transmitter system thus also features potentially higher sensitivity to dispersive subsurface anomalies, which have been found to be a strong hydrocarbon indicator (Davydycheva *et al.* 2006).

First, for a range of CCMs, we want to assess the degree of accuracy that is achieved by their corresponding Debye series. The dispersive layer in Fig. 8 is described by the constant CCM parameters $m = 0.2$, $\tau = 10$. Transients at different offsets are computed for the three CCM exponents 1, 0.5 and 0.25. Each instance for offset and c-parameter in Fig. 9 contains (1) the digital-filter solution calculated from the actual CCM (eq. 1) (black dots), (2) the digital-filter solution of the corresponding Debye series (eq. 10) (red lines), and (3) the (Debye series) FDTD calculation (blue lines). In the following, these three solutions are referred to as, respectively, $\mathrm{DF}_{\mathrm{CCM}}$, $\mathrm{DF}_{\mathrm{Debye}}$ and FDTD. Vertical electric fields are generated through a turn-off source waveform, involving eqs (12) and (18) for the FDTD runs. To gauge the magnitude of the IP effect, Fig. 9 also contains the non-IP fields (grey lines).

Two difference measures are calculated for each case and quantified as per cent values in corresponding subplots in Fig. 10. The first difference, $\Delta(\mathrm{FDTD}, \mathrm{DF}_{\mathrm{CCM}})$, is between FDTD and CCM reference and attempts to assess the quality of the FDTD solution using the updating scheme eq. (18). The second difference, $\Delta(\mathrm{DF}_{\mathrm{Debye}}, \mathrm{DF}_{\mathrm{CCM}})$, is between the two transformed frequency-domain solutions and attempts to isolate the error due to the Debye approximation. Note that spiking differences coincide with sign reversals in the transients of Fig. 9. Deviations between different numerical solutions are typical near sign reversals (Commer & Newman 2004). Apart from those, visual inspection of Fig. 9 indicates a qualitatively good agreement between FDTD outcome and the reference $\mathrm{DF}_{\mathrm{CCM}}$. An excellent match exists between all solution types at the largest offset (Rx3). However, the goodness of fit deteriorates with decreasing receiver offset. This

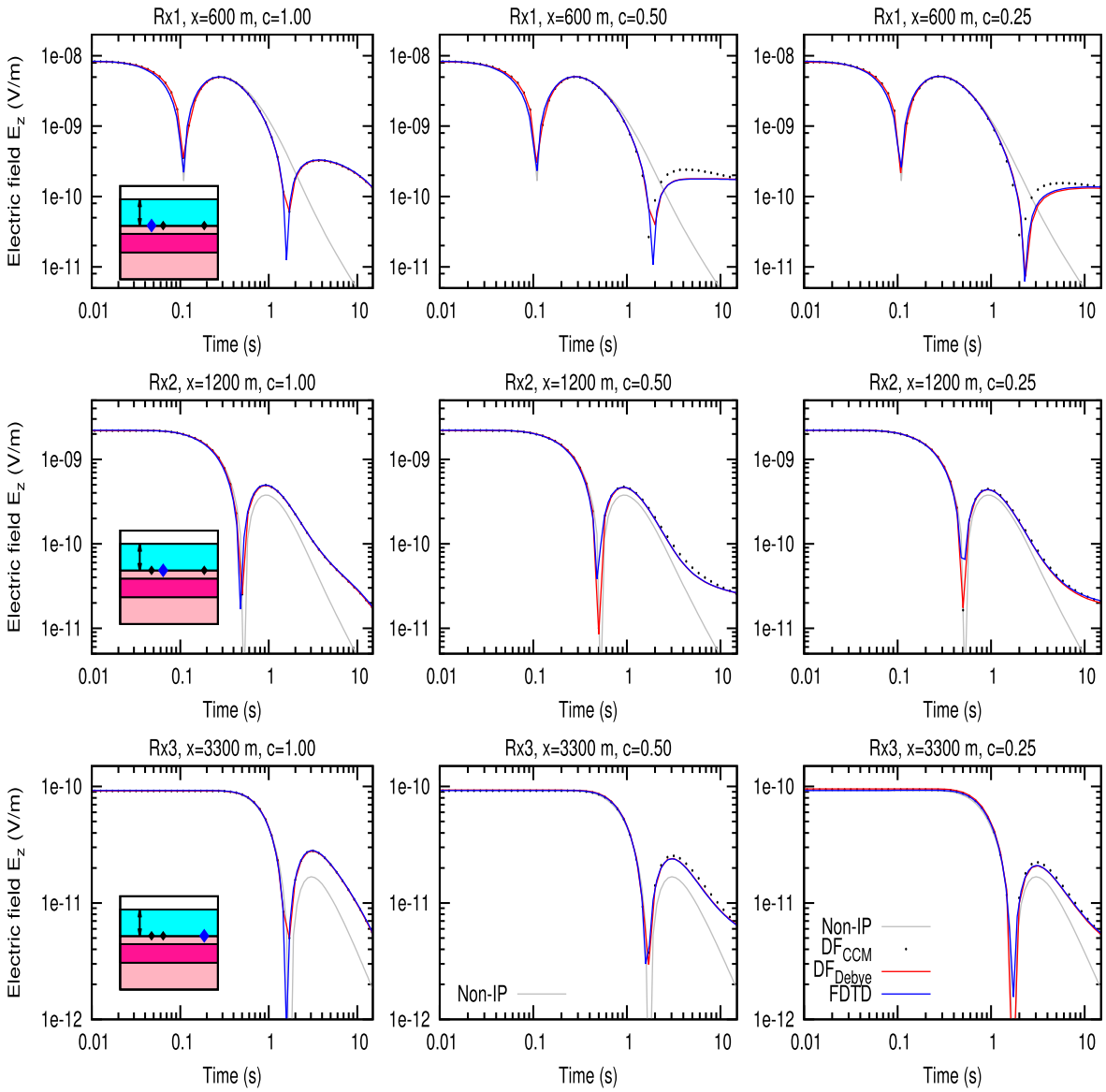

Figure 9. Vertical electric field transients calculated for the marine deep-water model of Fig. 8. For each of the three sampled receiver positions, the CCM exponent is varied between the values 1, 0.5 and 0.25. For each instance, transformed frequency-domain reference solutions (DF) are calculated for both the actual CCM (black dots) and the corresponding Debye series (red lines). These are to be compared to both the non-dispersive (grey lines) and dispersive FDTD responses (blue lines).

observation also agrees with our experience that conforming far-field solutions of different numerical EM schemes tend to diverge with decreasing transmitter-receiver distances. Finally, the differences in Fig. 10 reveal that the disagreement between FDTD and digital filter solution is dominated by the error due to the Debye-series approximation. Apart from the transient times near sign reversals, both errors $\Delta(\text{FDTD}, \text{DF}_{\text{CCM}})$ and $\Delta(\text{DF}_{\text{Debye}}, \text{DF}_{\text{CCM}})$ roughly agree for all instances.

3.5 Surface 3-D model

The final model study focuses on investigating the limitations on the accuracy of computing TEM signal anomalies due to shallow IP effects. Fig. 11 shows a representative land-based 3-D model, where only anomalous CCM parameters are considered, that is, the conductivity describes a homogeneous half-space at $\sigma = 1$ S m^{-1}. The parameters $\sigma_0 = 1$ S m^{-1}, $m = 0.1$, $\tau = 1$ s and three instances of c ($c_1 = 0.25$, $c_2 = 0.5$ and $c_3 = 0.75$) define the dispersivity of an anomalous block located at depth 300 m and with a size of 400 m $\times$ 800 m $\times$ 300 m. A horizontal electric dipole transmitter generates the TEM field, where the horizontal electric component is calculated along two surface profiles.

Fig. 12(a) exemplifies the dispersive versus non-dispersive response at the sample location $x = -900$ m along the transmitter line. In order to obtain a reference for the dispersive FDTD response (annotated as IP FDTD), we calculated 3-D frequency-domain responses

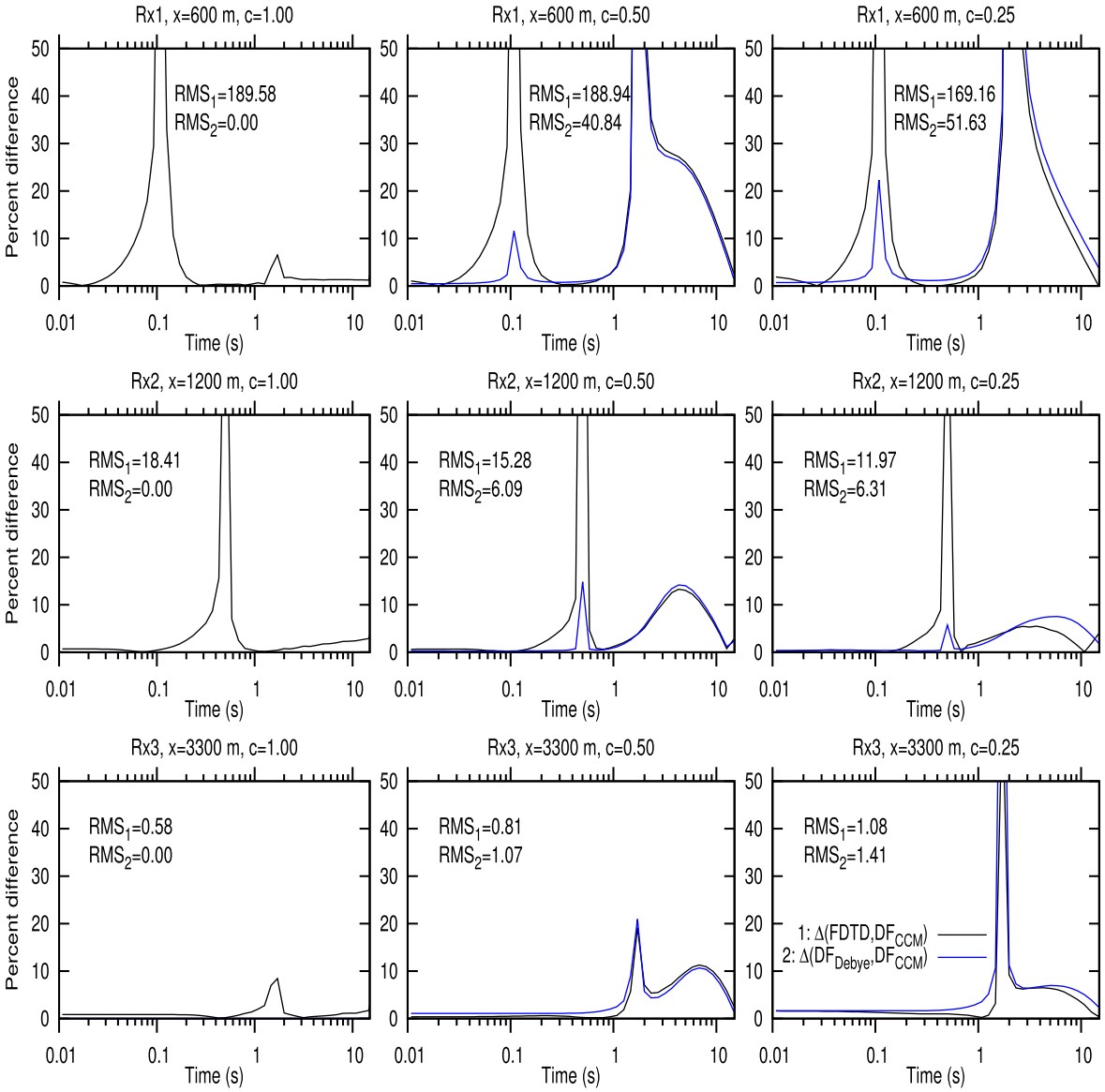

Figure 10. Per cent differences between vertical electric field transients calculated for the marine deep-water model of Fig. 8. Each subplot corresponds to the same receiver position and CCM exponent combination shown in Fig. 9. The first difference (black lines) is between FDTD and transformed frequency-domain reference calculated from the true CCM. The second difference (blue lines) is between both transformed frequency-domain solutions (Debye series versus true CCM). Further annotated are the RMS values for both differences. Note that $\Delta(\mathrm{DF}_{\mathrm{Debye}}, \mathrm{DF}_{\mathrm{CCM}}) = 0$ for $c = 1$.

for 71 logarithmically sampled frequencies of the band $[2.12 \times 10^{-4}, 9.86]$ Hz, using a frequency-domain finite-difference scheme with Krylov-solver technique (Commer & Newman 2008). The same digital-filter technique as used earlier transformed these field calculations into the time-domain (annotated as IP DF). Visually, the two transients agree well in revealing the slowed-down transient decay, in comparison to the non-IP response.

Being interested in the quantification of the numerical modelling error, we use two RMS measures of the form

$$\mathrm{RMS} = \sqrt{\frac{1}{N}\sum_{i=1}^{i=N}\left(\frac{\Delta_i}{\delta_i}\right)^2},$$

where $N = 38$ times are sampled over the logarithmic time range shown in Fig. 12(a). For the first measure, Δ_i is calculated from the difference between both FDTD solutions (no-IP versus IP). This serves as an estimate for the actual magnitude due to the polarizable media. For the second measure, Δ_i is calculated from the difference between both dispersive solutions (IP FDTD versus IP DF). This measure is an estimate for the numerical accuracy, in relation to the IP effect's magnitude. Both measures use the standard deviation of $\delta_i = d_i \times 0.01$, which is 1 per cent of the E_x-field samples d_i calculated from the non-dispersive FDTD simulation. Figs 12(b) and (c) show these RMS errors sampled along the receiver profiles at $y = 0$ m and $y = 400$ m, respectively. To see the numerical error (annotated as Δ) resulting from the two different

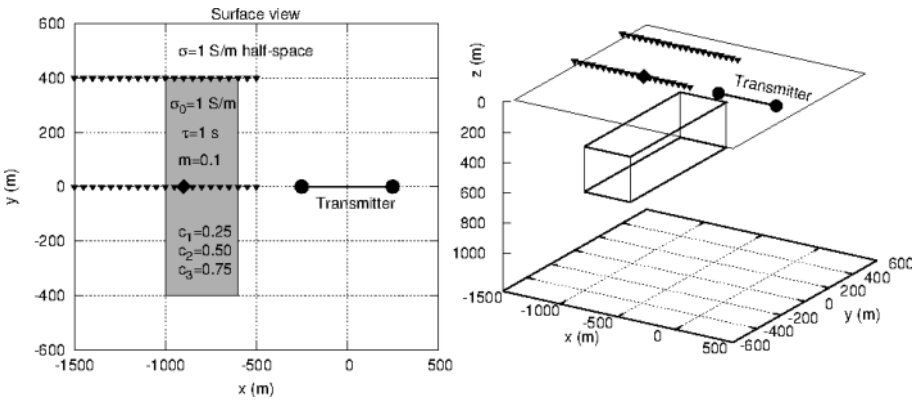

Figure 11. 3-D model of a land-based TEM survey over a shallow dispersive anomaly at a depth of 300 m. Two receiver profiles cross the block's centre and edge. Simulated are horizontal electric fields excited by a horizontal line source at the surface ($z = 0$ m).

3-D simulations in relation to the degree of the dispersive anomaly (annotated as IP magnitude), compare the curve pairs given for a specific exponent c, for example, the light and dark blue curves related to $c_2 = 0.5$.

For this configuration, the IP phenomenon is most pronounced along the profile range starting at roughly 200 m away from the block's left edge ($x = -1200$ m) and ending at approximately 700 m ($x = -700$ m) away from the source. Along this section, both profiles let us deduce roughly an order of magnitude difference between the two RMS measures. Generally, the sensitivity to the polarizable anomaly is larger over the central profile. Note that the IP effect vanishes near the right block edge ($x = -600$ m). Further, for the central profile, the numerical error owing to the grid discretization in the source vicinity increases towards the origin ($x = y = 0$).

In a field scenario, with the replication of 3-D IP effects being a computationally complex process, this method would help to estimate a threshold for the spatial delineation of IP anomalies. For example, anomalies in question that would be observed beyond $x = -1300$ m (moving away from the origin) are outside of the trust region. The trust region is defined by the dispersive field anomaly being sufficiently above the maximum numerical error of RMS ≈ 3 estimated for this profile location.

4 CONCLUSIONS

This work advances the FDTD method through the capability to simulate TEM signals containing IP phenomena from arbitrarily complex distributions of dispersive media described by the commonly used CCM. We first augmented the explicit FDTD time-stepping scheme by series of convolution terms that approximate a continuous relaxation time distribution in the form of quasi-equivalent multipole Debye models. The exponent c is the defining parameter for the number of Debye poles necessary to accurately match reference solutions calculated from arbitrary CCM dispersivity. Generally, the number of poles needs to increase with decreasing c. The replacement of exponential functions in the discrete-time convolution terms by composite memory variables is key in keeping reasonable FDTD runtimes.

The task of assessing the numerical accuracy of FDTD solutions due to dispersive media is not simple. First, the Debye-series approach suffers from a certain approximation error, which further escalates with the CCM's vanishing exponential function behaviour at low exponents. Second, how this error propagates into the late-time transient response, where the major part of the IP effect actually manifests, is not straightforward to answer. Lastly, the frequency-domain solutions that were employed in order to obtain a base for credible references, suffer from their own error sources inherent in the frequency-to-time transformation process. Our marine deep-water study indicated that for $c < 1$, the Debye-series approximation error dominates, because both FDTD and digital-filter Debye-series outcome revealed a similar deviation from the CCM reference. Nevertheless, the good agreement with the CCM reference solutions produced in all presented modelling examples supports the validity of the Debye-series approximation.

In the context of marine TEM data inversion, Holten *et al.* (2010) note that the optimal receiver offset is the threshold at which IP effects become negligible. This may not always be feasible, necessitating the inclusion of IP in inverse modelling. Therefore, the finding that weak dispersive responses can to first order be construed by (one-pole) Debye models may help to reduce the exasperating non-uniqueness problem that multipole Debye models would pose in 3-D inverse modelling attempts. We acknowledge that the curve-fitting implementation employed for this finding, together with the optimization method used for estimating Debye-series parameters, are rather rudimentary in terms of addressing the particular nature of the CCM function. Nevertheless, the multitude of modelling scenarios presented here show that a good range of CCM parameters with relevance to field surveys can already be covered with the presented methodology.

ACKNOWLEDGEMENTS

Funding for this work was provided by PetroMarker AS Norway. This material is also based upon research supported by the U.S. Department of Energy, Office of Science, Office of Basic Energy Sciences, Chemical Sciences, Geosciences, and Biosciences Division

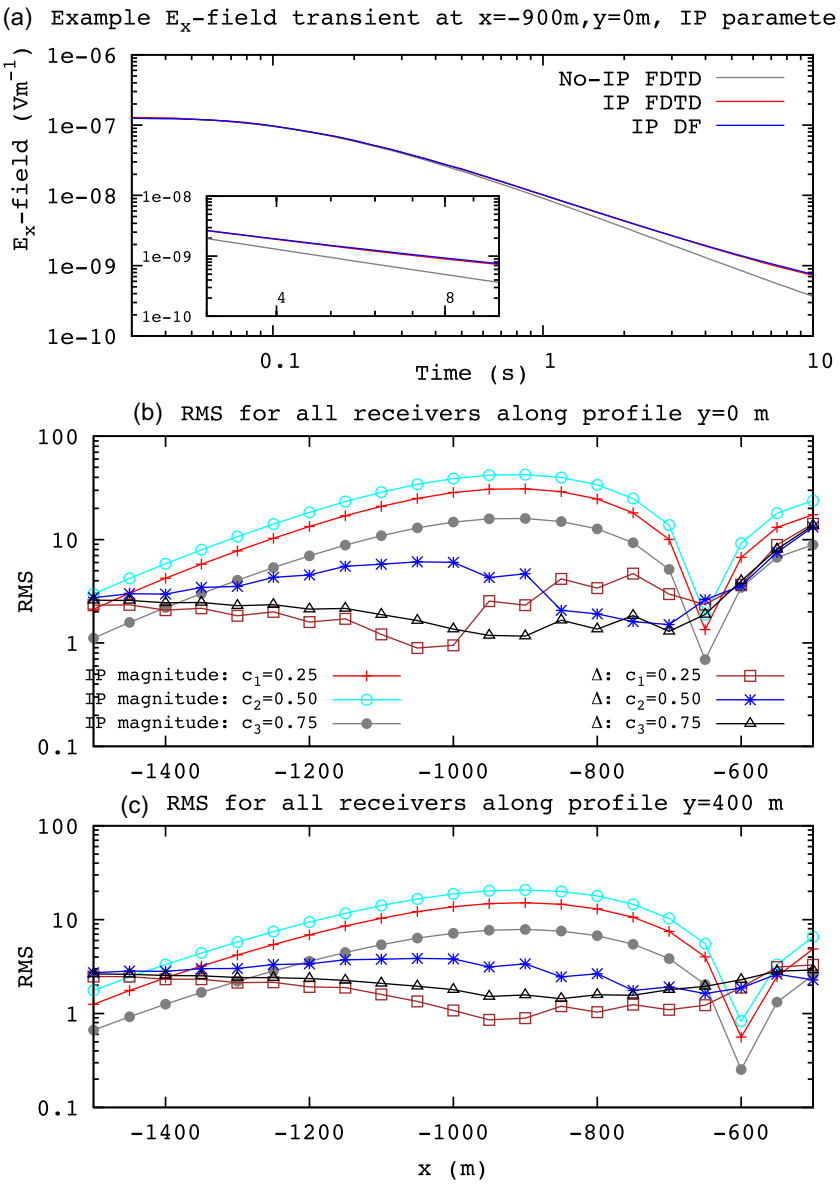

Figure 12. Horizontal TEM fields along the two receiver profiles above a 3-D dispersive anomaly. (a) Non-dispersive and dispersive FDTD transients and the corresponding digital-filter (DF) reference solution are exemplified for the example position marked by the large symbol in Fig. 11. For three different exponents c, RMS differences between non-IP and IP outcome quantify the magnitude of the IP effect. The set is accompanied by a comparison set of RMS differences between FDTD and reference (DF) calculations. Both RMS measures are sampled along (b) the central profile and (c) the profile over the body's edge.

under Contract DE-AC02-05CH11231. We also express our gratitude to two anonymous reviewers who helped to enhance the quality of this work.

REFERENCES

Abramowitz, M. & Stegun, I.A., 1972. *Handbook of Mathematical Functions with Formulas, Graphs, and Mathematical Tables,* 10th edn, Applied Mathematics Series 55, Dover Publications.

Carcione, J.M., 1990. Wave propagation in anisotropic linear viscoelastic media, *Geophys. J . Int.,* **101,** 739–750.

Carcione, J.M., Kosloff, D. & Kosloff, R., 1988. Wave propagation in a linear viscoacoustic medium, *Geophys. J.,* **93,** 393–407.

Chave, A.D., 1983. Numerical integration of related Hankel transforms by quadrature and continued fraction expansion, *Geophysics,* **48,** 1671–1686.

Commer, M. & Newman, G.A., 2004. A parallel finite-difference approach for 3D transient electromagnetic modeling with galvanic sources, *Geophysics,* **69,** 1192–1202.

Commer, M. & Newman, G.A., 2008. New advances in three-dimensional controlled-source electromagnetic inversion, *Geophys. J. Int.,* **172,** 513–535.

Commer, M., Hoversten, G.M. & Um, E.S., 2016. Transient-electromagnetic finite-difference time-domain earth modeling over steel infrastructure, *Geophysics,* **80,** E147–E162.

Davydycheva, S., Rykhlinski, N. & Legeido, P., 2006. Electrical-prospecting method for hydrocarbon search using the induced-polarization effect, *Geophysics,* **71,** G179–G189.

Emmerich, H. & Korn, M., 1987. Incorporation of attenuation into time-domain computations of seismic wave fields, *Geophysics,* **52,** 1252–1264.

Fiandaca, G., Auken, E., Gazoty, A. & Christiansen, A.V., 2012. Time-domain induced polarization: full-decay forward modeling and 1D

laterally constrained inversion of Cole-Cole parameters, *Geophysics,* **77,** E213–E225.

Flis, M.F., Newman, G.A. & Hohmann, G.W., 1989. Induced-polarization effects in time-domain electromagnetic measurements, *Geophysics,* **54,** 514–523.

Gandhi, O.P., Gao, B.Q. & Chen, J.Y., 1993. A frequency-dependent finite-difference time-domain formulation for general dispersive media, *IEEE Trans. Microw. Theory Tech.,* **41,** 658–665.

Holten, T., Flekkøy, E.G., Singer, B., Blixt, E.M., Hanssen, A. & Måløy, K.J., 2009. Vertical source, vertical receiver, electromagnetic technique for offshore hydrocarbon exploration, *First Break,* **27,** 89–93.

Holten, T., Singer, B. & Flekkøy, E.G., 2010. Effects of a limited reservoir and induced polarization on acquisition with vertical electrodes, *SEG Technical Program Expanded Abstracts*, pp. 874–878.

Hurt, W.D., 1985. Multiterm Debye dispersion relations for permittivity of muscle, *IEEE Trans. Biomed. Eng.,* **BME-32,** 60–64.

Kashiva, T., Ohtomo, Y. & Fukai, I., 1990. A finite-difference time-domain formulation for transient propagation in dispersive media associated with Cole-Cole's circular arc law, *Microw. Opt. Technol. Lett.,* **3,** 416–419.

Kelley, D.F. & Luebbers, R.J., 1996. Piecewise linear recursive convolution for dispersive media using FDTD, *IEEE Trans. Antennas Propag.,* **44,** 792–797.

Kelley, D.F., Destan, T.J. & Luebbers, R.J., 2007. Debye function expansions of complex permittivity using a hybrid particle swarm - least squares optimization approach, *IEEE Trans. Antennas Propag.,* **55,** 1999–2005.

Krewer, F., Morgan, F. & O'Halloran, M., 2013. Development of accurate multi-pole Debye functions for electromagnetic tissue modelling using a genetic algorithm, *Prog. Electromagn. Res. Lett.,* **43,** 137–147.

Lee, T., 1981. Short Note: The Cole-Cole model in time domain induced polarization, *Geophysics,* **46,** 932–933.

Luebbers, R.J., Hunsberger, F.P., Kunz, K.S., Standler, R.B. & Schneider, M., 1990. A frequency-dependent finite-difference time-domain formulation for dispersive materials, *IEEE Trans. Electromagn. Compat.,* **32,** 222–227.

Luebbers, R.J. & Hunsberger, F.P., 1992. FDTD for Nth-order dispersive media, *IEEE Trans. Antennas Propag.,* **40,** 1297–1301.

Marchant, D., Haber, E. & Oldenburg, D.W., 2014. Three-dimensional modeling of IP effects in time-domain electromagnetic data, *Geophysics,* **79,** E303–E314.

Moré, J.J., Sorensen, D.C., Hillstrom, K.E. & Garbow, B.S., 1984. The MINPACK Project, in *Sources and Development of Mathematical Software,* pp. 88–111, ed. Cowell, W.J., Prentice-Hall.

Nelder, A. & Mead, R., 1965. A simplex method for function minimization, *Comput. J.,* **7,** 308–313.

Newville, M., Stensitzki, T., Allen, D.B. & Ingargiola, A., 2014. 'LMFIT: Non-Linear Least-Square Minimization and Curve-Fitting for Python'. Available at: http://dx.doi.org/10.5281/zenodo.11813.

Nordsiek, S. & Weller, A., 2008. A new approach to fitting induced-polarization spectra, *Geophysics,* **73,** F235–F245.

Oristaglio, M.L. & Hohmann, G.W., 1984. Diffusion of electromagnetic fields into a two-dimensional earth: a finite-difference approach, *Geophysics,* **49,** 870–894.

Pelton, W.H., Ward, S.H., Hallof, P.G., Sill, W.R. & Nelson, P.H., 1978. Mineral discrimination and removal of inductive coupling with multifrequency IP, *Geophysics,* **43,** 588–609.

Petropoulos, P.G., 2008. Uniform in time asymptotic and numerical methods for propagation in dielectrics exhibiting fractional relaxation, and efficient and accurate impedance boundary conditions for high-order numerical schemes for the time-dependent Maxwell equations, *Techn. Report No. 20080404121*, Air Force Office of Scientific Research/NE.

Rekanos, I. & Papadopoulos, T., 2010. An auxiliary differential equation method for FDTD modeling of wave propagation in Cole-Cole dispersive media, *IEEE Trans. Antennas Propag.,* **58,** 3666–3674.

Revil, A. & Florsch, N., 2010. Determination of permeability from spectral induced polarization in granular media, *Geophys. J. Int.,* **181,** 1480–1498.

Revil, A., Florsch, N. & Camerlynck, C., 2014. Spectral induced polarization porosimetry, *Geophys. J. Int.,* **198,** 1016–1033.

Schmutz, M., Revil, A., Vaudelet, P., Batzle, M., Viñao, P.F. & Werkema, D.D., 2010. Influence of oil saturation upon spectral induced polarization of oil-bearing sands, *Geophys. J. Int.,* **183,** 211–224.

Schuster, J.W. & Luebbers, R.J., 1998. An FDTD algorithm for transient propagation in biological tissue with a Cole-Cole dispersion relation, in *Proceedings of IEEE Antennas Propagation Society International Symposium,* Jun. 21–26, 1998, vol. 4, pp. 1988–1991, doi:10.1109/APS.1998.701597.

Seigel, H.O., Nabighian, M., Parasnis, D.S. & Vozoff, K., 2007. The early history of the induced polarization method, *Leading Edge,* **26,** 312–321.

Sheppard, R.J., 1973. The least-squares analysis of complex weighted data with dielectric applications, *J. Phys. D: Appl. Phys,* **6,** 790–794.

Smith, R.S., Walker, P.W., Polzer, B.D. & West, G.F., 1988. The time-domain electromagnetic response of polarizable bodies: an approximate convolution algorithm, *Geophys. Prospect.,* **36,** 772–785.

Sullivan, D., 1992a. Frequency-dependent FDTD methods using z transforms, *IEEE Trans. Antennas Propagat.,* **40,** 1223–1230.

Sullivan, D., 1992b. A frequency-dependent FDTD method for biological applications, *IEEE Trans. Microw. Theory Tech.,* **40,** 532–539.

Taflove, A., Hagness, S., Gwarek, W., Fujii, M. & Chang, S.-H., 2005. Dispersive, nonlinear, and gain materials, in *Computational Electrodynamics, the Finite-Difference Time-Domain Method,* pp. 353–406, eds Taflove, A. & Hagness, S., 3rd edn, Artech House.

Tarasov, A. & Titov, K., 2007. Relaxation time distribution from time domain induced polarization measurements, *Geophys. J. Int.,* **170,** 31–43.

Tarasov, A. & Titov, K., 2013. On the use of the Cole-Cole equations in spectral induced polarization, *Geophys. J. Int.,* **195,** 352–356.

Teixeira, F.L., Chew, W.C., Straka, M., Oristaglio, M.L. & Wang, T., 1998. Finite-difference time-domain simulation of ground penetrating radar on dispersive, inhomogeneous, and conductive soils, *IEEE Trans. Geosci. Remote Sens.,* **36,** 1928–1937.

Torres, F., Vaudon, P. & Jecko, B., 1996. Application of fractional derivatives to the FDTD modeling of pulse propagation in a Cole-Cole dispersive medium, *Microw. Opt. Tech. Lett.,* **13,** 300–304.

Ustra, A., Mendonça, C.A., Ntarlagiannis, D. & Slater, L.D., 2016. Relaxation time distribution obtained from a Debye decomposition of spectral induced polarization data, *Geophysics,* **81,** E129–E138.

Wait, J.R., 1984. Relaxation phenomena and induced polarization, *Geoexploration,* **22,** 107–127.

Wang, T. & Hohmann, G.W., 1993. A finite-difference, time-domain solution for three-dimensional electromagnetic modeling, *Geophysics,* **58,** 797–809.

Weedon, W.H. & Rappaport, C.M., 1997. A general method for FDTD modeling of wave propagation in arbitrary frequency-dispersive media, *IEEE Trans. Antennas Propag.,* **45,** 401–410.

Wismer, M.G. & Ludwig, R., 1995. An explicit numerical time domain formulation to simulate pulsed pressure waves in viscous fluids exhibiting arbitrary frequency power law attenuation, *IEEE Trans. Ultrason. Ferroelectr. Freq. Control,* **42,** 1040–1049.

Xu, T. & McMechan, G.A., 1995. Composite memory variables for viscoelastic synthetic seismograms, *Geophys. J. Int.,* **121,** 634–639.

Zaslavsky, M. & Druskin, V., 2010. Solution of time-convolutionary Maxwell's equations using parameter-dependent Krylov subspace reduction, *J. Comput. Phys.,* **229,** 4831–4839.

APPENDIX A: FDTD ELECTRIC FIELD UPDATING SCHEMES FOR DISPERSIVE MEDIA

A1 Derivation for the turn-off source waveform

We first restate the Debye function expansion for the current density linked to the turn-off source waveform (eq. 12),

$$\mathbf{j}_{\text{off}} = \boldsymbol{\sigma}_\infty \mathbf{e}(t) + (\boldsymbol{\sigma}_0 - \boldsymbol{\sigma}_\infty)\mathbf{e}_{\text{DC}} \sum_{i=0}^{N_{\text{Debye}}} \alpha_i \exp\left(-\frac{t}{\tau_i}\right) + (\boldsymbol{\sigma}_0 - \boldsymbol{\sigma}_\infty) \sum_{i=0}^{N_{\text{Debye}}} \frac{\alpha_i}{\tau_i} \int_0^t \exp\left(-\frac{t-t'}{\tau_i}\right)\mathbf{e}(t')\mathrm{d}t'. \tag{A1}$$

For the initial conditions at $t = 0$, (A1) becomes

$$\mathbf{j}_{\text{off}} = \boldsymbol{\sigma}_\infty \mathbf{e}(0) + (\boldsymbol{\sigma}_0 - \boldsymbol{\sigma}_\infty)\mathbf{e}_{\text{DC}} = \boldsymbol{\sigma}_0 \mathbf{e}_{\text{DC}},$$

since $\mathbf{e}(0) = \mathbf{e}_{\text{DC}}$ and assuming that $\sum_{i=0}^{N_{\text{Debye}}} \alpha_i = 1$ holds for the Debye series representation in eq. (A1). The electric field updating scheme is based on the following FD representation of Ampere's law (eq. 4), here in its FD representation (Wang & Hohmann 1993; Commer & Newman 2004):

$$\gamma \frac{\mathbf{e}^{n+1} - \mathbf{e}^n}{\Delta t} + \frac{\mathbf{j}^n + \mathbf{j}^{n+1}}{2} = \nabla \times \mathbf{h}^{n+\frac{1}{2}} - \mathbf{j}_s^{n+\frac{1}{2}}, \tag{A2}$$

where $\mathbf{j}^n$ and $\mathbf{j}^{n+1}$ denote the current density given by eq. (A1) at the current time step n and at the time step $n+1$ to be updated,

$$\mathbf{j}^n = \boldsymbol{\sigma}_\infty \mathbf{e}^n + (\boldsymbol{\sigma}_0 - \boldsymbol{\sigma}_\infty) \sum_{i=0}^{N_{\text{Debye}}} \alpha_i \exp\left(-\frac{t^n}{\tau_i}\right)\mathbf{e}_{\text{DC}} + (\boldsymbol{\sigma}_0 - \boldsymbol{\sigma}_\infty) \sum_{i=0}^{N_{\text{Debye}}} \frac{\alpha_i}{\tau_i} \int_0^{t^n} \exp\left(-\frac{t^n - t'}{\tau_i}\right)\mathbf{e}(t')\mathrm{d}t',$$

$$\mathbf{j}^{n+1} = \boldsymbol{\sigma}_\infty \mathbf{e}^{n+1} + (\boldsymbol{\sigma}_0 - \boldsymbol{\sigma}_\infty) \sum_{i=0}^{N_{\text{Debye}}} \alpha_i \exp\left(-\frac{t^{n+1}}{\tau_i}\right)\mathbf{e}_{\text{DC}} + (\boldsymbol{\sigma}_0 - \boldsymbol{\sigma}_\infty) \sum_{i=0}^{N_{\text{Debye}}} \frac{\alpha_i}{\tau_i} \int_0^{t^{n+1}} \exp\left(-\frac{t^{n+1} - t'}{\tau_i}\right)\mathbf{e}(t')\mathrm{d}t'.$$

The expressions for $\mathbf{j}^n$ and $\mathbf{j}^{n+1}$ are now inserted into the FD scheme given by eq. (A2), leading to

$$\gamma \frac{\mathbf{e}^{n+1} - \mathbf{e}^n}{\Delta t} + \frac{1}{2}\Bigg\{\boldsymbol{\sigma}_\infty \mathbf{e}^n + \boldsymbol{\sigma}_\infty \mathbf{e}^{n+1} + (\boldsymbol{\sigma}_0 - \boldsymbol{\sigma}_\infty)\mathbf{e}_{\text{DC}} \sum_{i=0}^{N_{\text{Debye}}} \left[\exp\left(-\frac{t^n}{\tau_i}\right) + \exp\left(-\frac{t^{n+1}}{\tau_i}\right)\right]$$
$$+ (\boldsymbol{\sigma}_0 - \boldsymbol{\sigma}_\infty) \sum_{i=0}^{N_{\text{Debye}}} \frac{\alpha_i}{\tau_i}\left[\int_0^{t^n} \exp\left(-\frac{t^n - t'}{\tau_i}\right)\mathbf{e}(t')\mathrm{d}t' + \int_0^{t^{n+1}} \exp\left(-\frac{t^{n+1} - t'}{\tau_i}\right)\mathbf{e}(t')\mathrm{d}t'\right]\Bigg\} = \nabla \times \mathbf{h}^{n+\frac{1}{2}} - \mathbf{j}_s^{n+\frac{1}{2}}. \tag{A3}$$

We seek to replace the computationally prohibitive convolution integrals of eq. A3 (within brackets of the left-hand-side's last summation term) by a corresponding set of memory variables. This requires equalizing their integration limits. Splitting up the second integral into

$$\int_0^{t^{n+1}} \exp\left(-\frac{t^{n+1} - t'}{\tau_i}\right)\mathbf{e}(t')\mathrm{d}t' = \int_0^{t^n} \exp\left(-\frac{t^{n+1} - t'}{\tau_i}\right)\mathbf{e}(t')\mathrm{d}t' + \int_{t^n}^{t^{n+1}} \exp\left(-\frac{t^{n+1} - t'}{\tau_i}\right)\mathbf{e}(t')\mathrm{d}t',$$

the second summand, $\int_{t^n}^{t^{n+1}}\{\ldots\}$, can be evaluated, using $\Delta t = t^{n+1} - t^n$:

$$\int_{t^n}^{t^{n+1}} \exp\left(-\frac{t^{n+1} - t'}{\tau_i}\right)\mathbf{e}(t')\mathrm{d}t' = \left[\exp\left(\frac{-\Delta t}{\tau_i}\right)\mathbf{e}^n + \mathbf{e}^{n+1}\right]\frac{\Delta t}{2}.$$

The sum of the two convolution integrals in eq. (A3) (within brackets) then becomes

$$\int_0^{t^n} \exp\left(-\frac{t^n - t'}{\tau_i}\right)\mathbf{e}(t')\mathrm{d}t' + \left[\exp\left(\frac{-\Delta t}{\tau_i}\right)\mathbf{e}^n + \mathbf{e}^{n+1}\right]\frac{\Delta t}{2} + \int_0^{t^n} \exp\left(-\frac{t^n + \Delta t - t'}{\tau_i}\right)\mathbf{e}(t')\mathrm{d}t',$$

where t^{n+1} was replaced by $t^n + \Delta t$. Before inserting this expression into eq. (A3), we use the equality

$$\exp\left(-\frac{t^n + \Delta t - t'}{\tau_i}\right) = \exp\left(-\frac{t^n - t'}{\tau_i}\right) + \exp\left(-\frac{\Delta t}{\tau_i}\right),$$

which is the last step to obtain an updating equation suitable to replacing the convolution integrals by memory variables,

$$\gamma \frac{\mathbf{e}^{n+1} - \mathbf{e}^n}{\Delta t} + \frac{1}{2}\Bigg\{\boldsymbol{\sigma}_\infty \mathbf{e}^n + \boldsymbol{\sigma}_\infty \mathbf{e}^{n+1} + (\boldsymbol{\sigma}_0 - \boldsymbol{\sigma}_\infty)\mathbf{e}_{DC} \sum_{i=0}^{\text{Debye}} \left[\exp\left(-\frac{t^n}{\tau_i}\right) + \exp\left(-\frac{t^{n+1}}{\tau_i}\right)\right]$$
$$+ (\boldsymbol{\sigma}_0 - \boldsymbol{\sigma}_\infty) \sum_{i=0}^{\text{Debye}} \frac{\alpha_i}{\tau_i}\left[\left(\exp\left(-\frac{\Delta t}{\tau_i}\right)\mathbf{e}^n + \mathbf{e}^{n+1}\right)\frac{\Delta t}{2} + \int_0^{t^n} \exp\left(-\frac{t^n - t'}{\tau_i}\right)\mathbf{e}(t')\mathrm{d}t'\left[1 + \exp\left(-\frac{\Delta t}{\tau_i}\right)\right]\right]\Bigg\} = \nabla \times \mathbf{h}^{n+\frac{1}{2}} - \mathbf{j}_s^{n+\frac{1}{2}}. \tag{A4}$$

As outlined in Section 2.4, for each Debye pole i, an individual memory variable M_i^n replaces the convolution term

$$\int_0^{t^n} \exp\left(-\frac{t^n - t'}{\tau_i}\right)\mathbf{e}(t')\mathrm{d}t'$$

that is associated with this Debye pole through the parameters α_i and τ_i. Rearranging eq. (A4) for the new electric field, $\mathbf{e}^{n+1}$, that is be computed at time t^{n+1}, one finally obtains the updating scheme given by eq. (18), to be repeated here:

$$\begin{aligned}\mathbf{e}^{n+1} = &\left\{\mathbf{e}^n\left[\frac{\gamma}{\Delta t} - \frac{\boldsymbol{\sigma}_\infty}{2} + \frac{\boldsymbol{\sigma}_\infty - \boldsymbol{\sigma}_0}{4}\Delta t \sum_{i=0}^{N_{\text{Debye}}} \frac{\alpha_i}{\tau_i}\exp\left(-\frac{\Delta t}{\tau_i}\right)\right] + \mathbf{e}_{\text{DC}}\frac{\boldsymbol{\sigma}_\infty - \boldsymbol{\sigma}_0}{2}\left[\sum_{i=0}^{N_{\text{Debye}}} \alpha_i \exp\left(-\frac{t^{n+1}}{\tau_i}\right) + \alpha_i \exp\left(-\frac{t^n}{\tau_i}\right)\right]\right.\\ &\left. + \frac{\boldsymbol{\sigma}_\infty - \boldsymbol{\sigma}_0}{2}\sum_{i=0}^{N_{\text{Debye}}} \frac{\alpha_i}{\tau_i} M_i^n\left[1 + \exp\left(-\frac{\Delta t}{\tau_i}\right)\right] + \nabla \times \mathbf{h}^{n+\frac{1}{2}} - \mathbf{j}_s^{n+\frac{1}{2}}\right\} \Bigg/ \left(\frac{\gamma}{\Delta t} + \frac{\boldsymbol{\sigma}_\infty}{2} - \frac{\boldsymbol{\sigma}_\infty - \boldsymbol{\sigma}_0}{4}\Delta t \sum_{i=0}^{N_{\text{Debye}}} \frac{\alpha_i}{\tau_i}\right).\end{aligned} \tag{A5}$$

Each time step further involves accumulating all memory terms M_i

$$M_i^{n+1} = M_i^n\left(1 - \frac{\Delta t^n}{\tau_i}\right) + \mathbf{e}^n \Delta t. \tag{A6}$$

A2 Derivation for the turn-on source waveform

Restating the Debye function expansion for the current density related to a turn-on source waveform (eq. 11),

$$\mathbf{j}_{\text{on}}(t) = \boldsymbol{\sigma}_\infty \mathbf{e}(t) + (\boldsymbol{\sigma}_0 - \boldsymbol{\sigma}_\infty)\sum_{i=0}^{N_{\text{Debye}}} \frac{\alpha_i}{\tau_i}\int_0^t \exp\left(-\frac{t - t'}{\tau_i}\right)\mathbf{e}(t')\mathrm{d}t',$$

one notes that it differs from eq. (A1) only by the vanishing term associated with the DC electric field. Hence, the derivation of the electric field updating scheme is almost identical to Appendix A1. By omitting the DC terms in all steps that produce eqs (A3)–(A4), one obtains the final updating scheme for the turn-on source (eq. 17), rewritten here for completeness,

$$\begin{aligned}\mathbf{e}^{n+1} = &\left\{\mathbf{e}^n\left[\frac{\gamma}{\Delta t} - \frac{\boldsymbol{\sigma}_\infty}{2} + \frac{\boldsymbol{\sigma}_\infty - \boldsymbol{\sigma}_0}{4}\Delta t \sum_{i=0}^{N_{\text{Debye}}} \frac{\alpha_i}{\tau_i}\exp\left(-\frac{\Delta t}{\tau_i}\right)\right]\right.\\ &\left. + \frac{\boldsymbol{\sigma}_\infty - \boldsymbol{\sigma}_0}{2}\sum_{i=0}^{N_{\text{Debye}}} \frac{\alpha_i}{\tau_i} M_i^n\left[1 + \exp\left(-\frac{\Delta t}{\tau_i}\right)\right] + \nabla \times \mathbf{h}^{n+\frac{1}{2}} - \mathbf{j}_s^{n+\frac{1}{2}}\right\} \Bigg/ \left(\frac{\gamma}{\Delta t} + \frac{\boldsymbol{\sigma}_\infty}{2} - \frac{\boldsymbol{\sigma}_\infty - \boldsymbol{\sigma}_0}{4}\Delta t \sum_{i=0}^{N_{\text{Debye}}} \frac{\alpha_i}{\tau_i}\right).\end{aligned} \tag{A7}$$

This scheme also employs eq. (A6) for recalculating the memory terms M_i.

A last sidenote is that only Ampere's law is affected, that is, both Faraday's law of induction and Gauss's law of magnetism ($\nabla \cdot \mathbf{b} = 0$) retain the same formulations as for the non-dispersive case. Finally, a basic check considers the non-dispersive case, where $\boldsymbol{\sigma}_\infty = \boldsymbol{\sigma}_0 = \boldsymbol{\sigma}$, which collapses both eqs (A5) and (A7) to

$$\begin{aligned}\mathbf{e}^{n+1} &= \mathbf{e}^n\left[\left(\frac{\gamma}{\Delta t} - \frac{\boldsymbol{\sigma}}{2}\right) + \nabla \times \mathbf{h}^{n+\frac{1}{2}} - \mathbf{j}_s^{n+\frac{1}{2}}\right)\Bigg] \Bigg/ \left(\frac{\gamma}{\Delta t} + \frac{\boldsymbol{\sigma}}{2}\right)\\ &= \frac{2\gamma - \boldsymbol{\sigma}\Delta t}{2\gamma + \boldsymbol{\sigma}\Delta t}\mathbf{e}^n + \frac{2\Delta t}{2\gamma + \boldsymbol{\sigma}\Delta t}\left(\nabla \times \mathbf{h}^{n+\frac{1}{2}} - \mathbf{j}_s^{n+\frac{1}{2}}\right),\end{aligned}$$

which is in agreement with the non-dispersive updating formulation for the electric field given by eq. (16).